Crater clusters on Mars: Shedding light on martian ejecta launch conditions

Olga P. Popova [a,*], William K. Hartmann [b], Ivan V. Nemtchinov [a], Derek C. Richardson [c], Daniel C. Berman [b]

[a] *Institute for Dynamics of Geospheres, Russian Academy of Sciences, Leninsky Prospekt 38, Bldg. 1, 119334 Moscow, Russia*
[b] *Planetary Science Institute, 1700 East Fort Lowell Road, Suite 106, Tucson, AZ 85719-2395, USA*
[c] *University of Maryland, Stadium Drive, College Park, MD 20742-2421, USA*

Abstract

We have identified two classes of crater clusters on Mars. One class is "small clusters" (crater diameter $D \sim$ tens m, spread over few hundred m), fitting our earlier calculations for the breakup of weak stone meteoroids in the martian atmosphere [Popova, O.P., Nemtchinov, I.V., Hartmann, W.K., 2003. Meteorit. Planet. Sci. 38, 905–925]. The second class is "large clusters" ($D \sim$ few hundred m, spread over 2 to 30 km), which do not fit any predictions for breakup of known meteoroid types. We consider a range of possible explanations. The best explanation relates to known, high-speed ejection of large, semi-coherent, fractured rock masses from the surface, as secondary debris from primary impacts. The clusters are probably due to breakup of partly fracture, few-hundred-meter scale weak blocks, especially during ascent (producing moderate lateral spreading velocities among the fragments during sub-orbital flight), and also during descent of the resulting swarm. These conclusions illuminate the launch conditions of martian meteorites, including fragmentation processes, although more work is needed on the lateral separation of fragments (during either atmosphere descent or ascent) due to the effects of volatiles in the projectiles. Martian meteorites probably come from smaller martian craters than the clusters' source craters. The latter probably have $D \gtrsim 85$ km, although we have not ruled out diameters as small as 15 km.
© 2007 Elsevier Inc. All rights reserved.

Keywords: Cratering; Mars; Meteorites; Impact processes

1. Martian crater clusters

In a previous paper we examined the passage of meteoroids through the martian atmosphere, and predicted that weak stone meteorites, within the strength range of measured chondrites, would explode in the martian atmosphere and create clusters of craters on the margins of Mars Global Surveyor resolution, typically of diameter $D \sim 10$–20 m spread over regions a few hundred meters wide. We presented an example of such a feature (Popova et al., 2003); subsequently we have identified many more examples (Fig. 1). That type of feature appears common enough to confirm the general results of our modeling of bolides in the martian atmosphere, including fragmentation of certain sizes of weak stone bodies.

Our earlier work began, however, with examination of a different type of crater cluster which could not be explained by the earlier modeling. These are clusters of much larger craters, found during examination of Viking pictures prior to the Mars Global Surveyor mission. They are numerous and seemingly isolated clusters of craters with D mostly ~ 70 to 900 m. The clusters are typically 2 to 30 km wide (Hartmann and Engel, 1994). Examples are shown in Figs. 2–6 they show a range of morphologies. Many of them (Figs. 2, 3, 5, and 6) show overlapping pits in areas 5–10 km wide, while at the other end of the spectrum (Fig. 4) there are widely separated individual craters, strewn over areas 30 km wide or more.
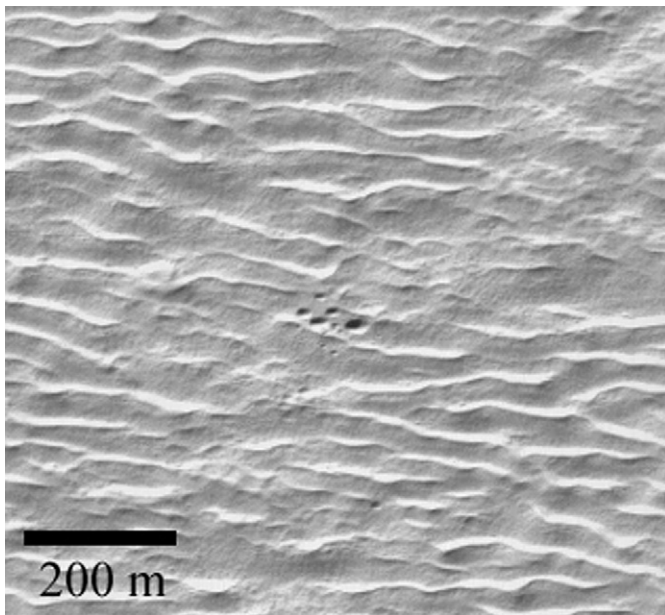
Our figures include crater counts that show peaking in the size distribution, atypical of ordinary background craters. Fig. 5 is a good example. It is our highest latitude example and appears to mantled by the deposits described by Mustard et al.
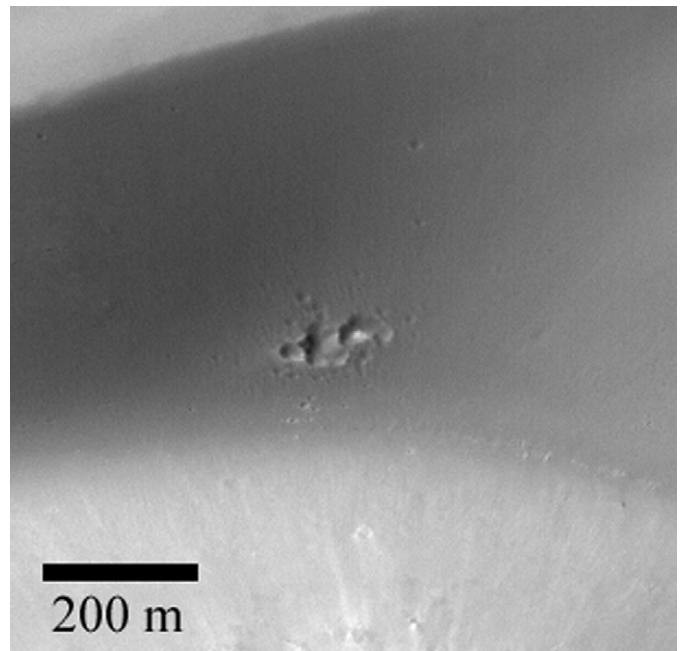
* Corresponding author.
  E-mail address: olga@idg.chph.ras.ru (O.P. Popova).
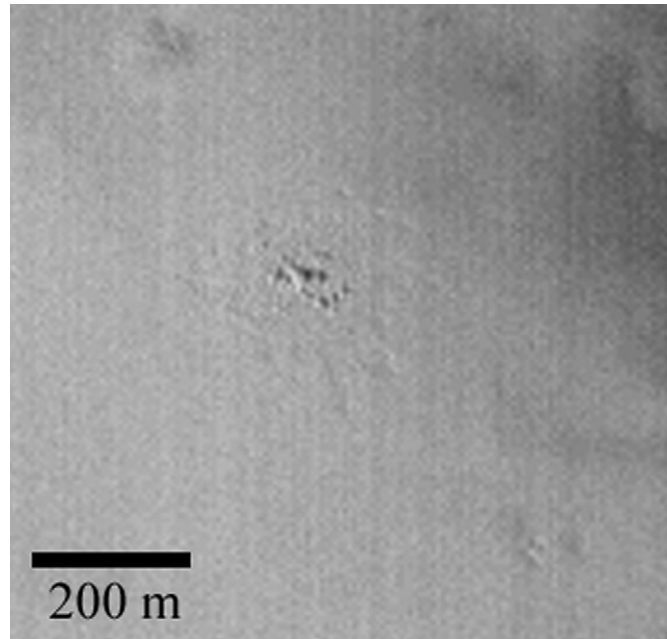
(a)

(b)

(c)

Fig. 1. Examples of "small crater clusters" where craters have diameter *D* of order 10 m and clusters spread over area roughly 100 m across. These clusters fit the predictions of Popova et al. (2003) for breakup of weak stone bolides in the present atmosphere of Mars. The clusters appear distinct from the "large crater clusters" discussed in the present paper. (a) Cluster in featureless area in Arabia (323° W, 12° N; Mars Global Surveyor MGS/MOC frame M09-02052). (b) Cluster inside Newton (158° N, 45° S; MGS/MOC frame M19-00278). (c) Cluster on NE wall Bakhuysen Crater (343° W, 23° S; MGS/MOC frame M02-0763).

(2001). In Fig. 5c, unlike the other crater count figures, we present counts made to characterize the background surface as well as the cluster. It is notable that the crater counts show comparable crater densities in the mantled background and in the cluster itself at diameters $D < 500$–700 m (mostly within factor 2 and within error bars; the background appears slightly older), while the cluster stands out with much higher density at $D \sim 700$–2000 m. However, sharp, fresh-looking craters that appear to postdate mantle deposition appear to date the mantle

itself at a significantly younger model age, around 10–100 Myr, at least for accumulation of mantle depths capable of degrading the craters of $D = 22$–250 m (depths $\sim$7–70 m). In other words, the background surface and the cluster itself appear older than 10^9 yr but the mantling process has probably been operating within the last 10^7–10^8 yr.

Hartmann and Engel (1994) suggested clusters might represent either breakups of unusually weak (cometary?) bodies, or "SNCs that did not make it"—dissociating blocks of secondary
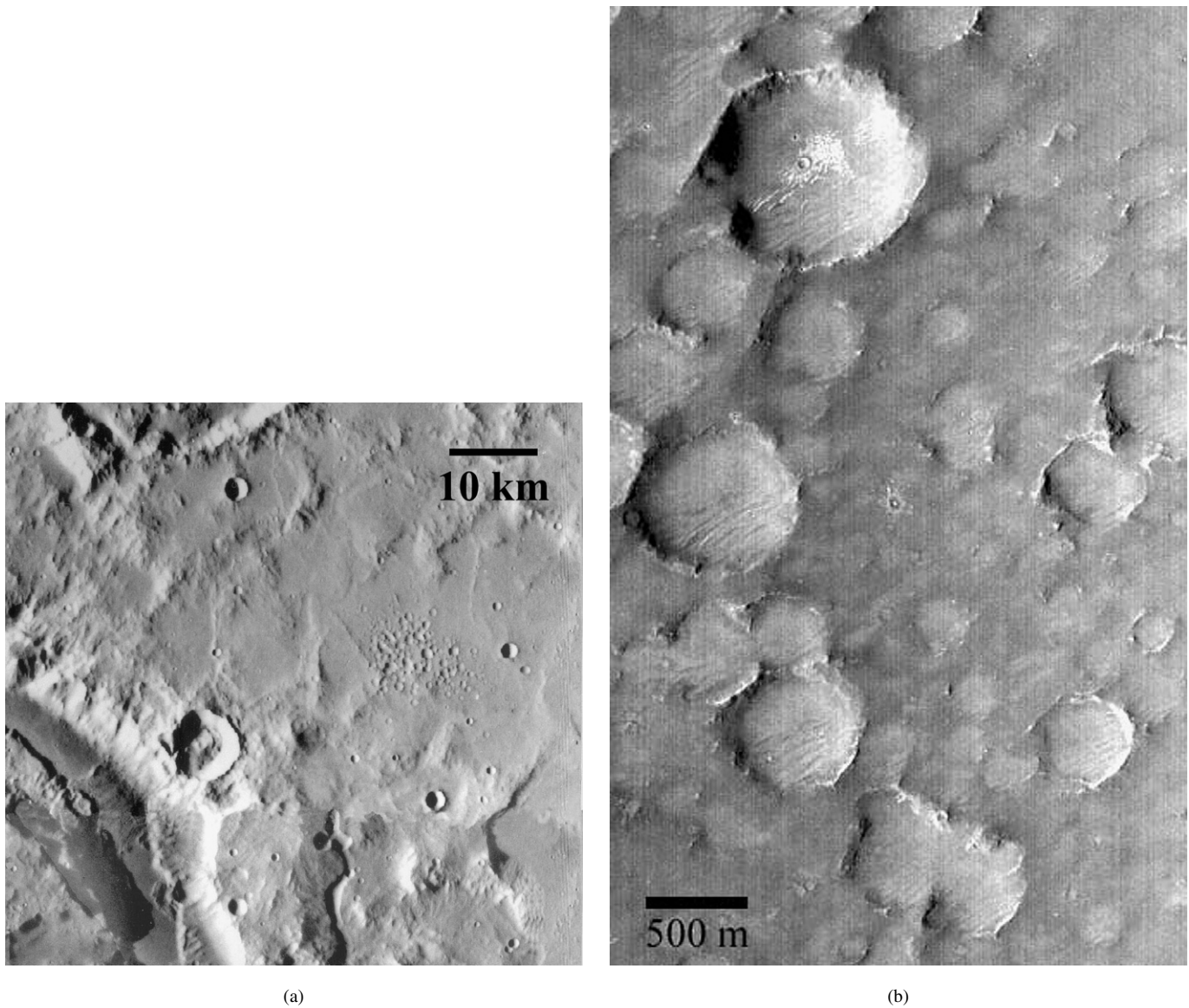
(a)

(b)

Fig. 2. Cluster near Ma'adim Vallis (182° W, 20° S). (a) Viking context image. Background is classified as Noachian cratered plateau unit (Greeley and Guest, 1987). (b) Detailed view; MGS/MOC M12-01425. Small craters appear degraded by later processes. (c) Crater counts indicating a peak in the size distribution at $160\ m \lesssim D \lesssim 500\ m$. Counts $D \sim 90$–$160\ m$ suggest the surface within the cluster may have age < 1 Gyr (i.e., the cluster may postdate the Noachian). The flattened curve at $D \lesssim 90\ m$, plus degraded morphologies, suggests gradual losses by infill, mantling, or other obliteration processes continuing into more recent times.

debris lofted into space but falling back to random spots on Mars. The first of these options raised the exciting possibility of detecting physical properties of a class of extremely weak, ice-rich, and/or loosely bound comets. Barlow and Osborne (2001) revisited the problem and cataloged clusters to separate those in strings aligned with primaries (i.e., identifiably secondaries) from "isolated clusters." They characterized their examples as mostly having craters 1–4 km in size, and gave examples with craters up to 25 km in size, making their examples larger than in our clusters. They found a preference for Hesperian and Noachian terrain for these clusters, and provisionally concluded that they formed by breakup of rubble-pile asteroids and "friable material" in once-thicker atmospheres. The problem, however, is that fragmentation events, even with explosive release of volatiles heated by entry phenomena, appear unlikely to achieve the necessary spreading velocities, according to cur-

rent theories (see more details in Section 3). Comets are apt to strike Mars at velocities higher than those of asteroids. Even a "slow" comet might hit Mars with velocity > 10 km/s, with a flight time after fragmentation of perhaps 10 s (allowing for the higher atmospheric scale height on Mars). For example, if fragments spread > 5 km in each direction from the center of mass during a liberal allowance of 10 s of flight time after a breakup, lateral speeds of > 500 m/s would have to be achieved. Higher velocities would create higher kinetic energies for explosions, but result in even less flight time. Popova et al. (2003) calculated typical spreading velocities more like 3 to 8 m/s from the center of mass, and up to 20 m/s for smaller fragments in the stress-induced breakup of rocky bodies. For a 5–10 s flight time, this would predict cluster diameters of the order 30 to 400 m, as observed (Fig. 1). Having cited these theoretical models, we must note that they do not
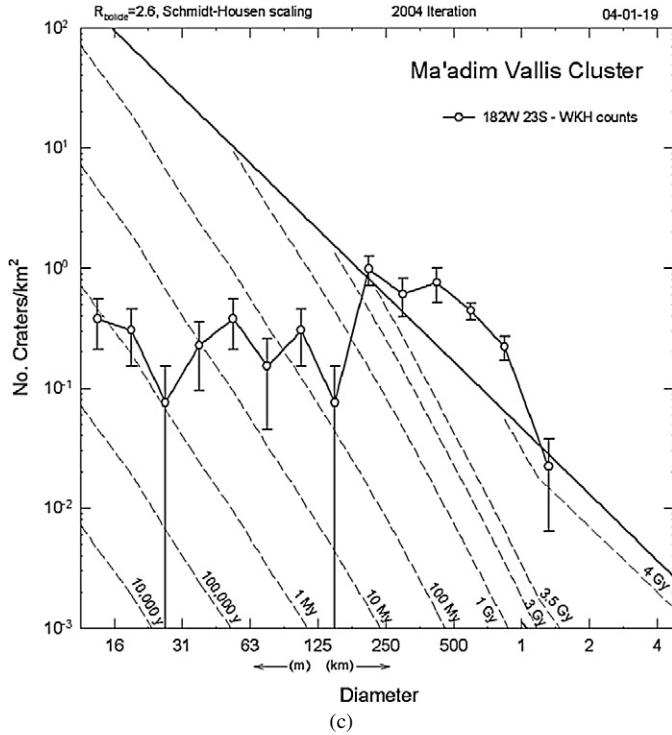
Fig. 2. (*continued*)

have detailed physics to represent the acceleration by exploding volatiles.

In any case, present understanding makes it unlikely that required spreading velocities of the order 500, 1000 m/s, or more could be achieved in breakup of interplanetary meteoroids during descent through the martian atmosphere. (See further discussion in Sections 2 and 3.) This leaves the origin of the larger clusters unknown. We investigate the problem here in the belief that these puzzling clusters may shed light on martian phenomena.

We have made preliminary searches in a number of these cases for nearby fresh, large, primary craters that could be sources of fields of secondary craters. The search is more difficult than on the moon because of erosional and depositional modification of primaries and their surroundings, but in most cases there is no obvious parent crater. Nearby primary craters, with massive swarms of secondaries and strings leading to our cluster examples, have not been identified in our Figs. 2–4. Nonetheless, craters with nearby secondary swarms and radial strings of secondaries do exist. Fig. 6 shows a full-fledged example of a string of secondaries with swarm width ∼3 to 5 km. McEwen et al. (2005) have pointed out a 10-km martian primary crater, Zunil, that has scattered secondary pits, many concentrated in rays and radial strings, over a wide region of Elysium Planitia, traceable out to a radial distance of 800–1600 km; McEwen et al. (2005) report that they range in diameter up to 230 m. These examples establish that secondary ejecta can spread laterally to the scatter-widths we observe in clusters and can form craters of the sizes we observe in clusters. Clearly, if fragmenting debris is lofted to escape velocity in order to produce martian meteorites (henceforth MMs) on Earth,

then other debris is lofted to barely suborbital speeds and secondary impact pits must exist not just in near-primary swarms, but also in near-random positions scattered around Mars.

According to crater ejecta scaling laws (Housen et al., 1983), volume A_{ej} ejected with velocity $V_{ej} > V$ is proportional to projectile volume A_p,

$$\frac{A_{ej}}{A_p} = \left\{ \frac{V\sqrt{2}}{\sqrt{gD}} \right\}^{\frac{6\alpha}{\alpha-3}}. \tag{1}$$

We may estimate the ratio of high velocity ejecta volume ($V >$ 1 km/s) to the SNC production volume ($V_{ej} > 5$ km/s):

$$\frac{A_{ej}}{A_{SNC}} = \left\{ \frac{V_{ej}}{V_{SNC}} \right\}^{\frac{6\alpha}{\alpha-3}}. \tag{2}$$

For a reasonable value of power constant $\alpha \sim 0.65$ (Housen et al., 1983; Holsapple, 1994), the amount of high velocity ejecta forming secondaries on the planet surface is about 13 times larger than A_{SNC}.

The numerical modeling of the MM launch (Artemieva and Ivanov, 2004) estimated the ratio of MM material volume ($V_{ej} > 5$ km/s) to the projectile ratio as about 0.024–0.105 for impact angles 60–30° to vertical and impact velocity 10 km/s. For a similar impact, the volume of high velocity ejecta ($V >$ 1 km/s) would be about 0.3–1.4 of projectile volume.

2. First-order observations and boundary conditions

2.1. Atmosphere

The clusters we discuss appear relatively young. Generally they are superimposed on other surface units of varied age, and do not appear to be heavily cratered by small (30-m scale), later impacts, although they often have still more recent dunes on their floors. Rims appear intact and sharp in many cases, even if the secondary craters themselves are irregular in shape. Rim surfaces are often relatively uncratered by new small primaries. In other cases the rims appear to be worn down or degraded, either by overlapping impact effects during cluster formation or by erosion and terrain-softening effects. We conclude that most of the clusters discussed here probably formed in the last half of martian time, not during the Noachian era. For this reason, we suspect they formed under essentially present-day, low-pressure atmospheric conditions.

We leave open an intriguing alternative. Transient periods of denser atmosphere are possible in principle in Hesperian or Amazonian time due to massive volcanism or obliquity changes, and clusters might have formed during these excursions (similar to the ideas of Barlow and Osborne, 2001). The maximum surface pressure P_S during such excursions is unknown. As will be discussed below, the clusters appear to be deficient in craters of $D \lesssim 80$ m to as much as 300 m in some cases, relative to the normal fragment or secondary crater size distributions, although some clusters appear to have a sparse population of later, smaller impact craters superimposed on them due to normal cratering after the cluster formed (Figs. 3b

Fig. 3. Cluster north of Isidis Planitia (270° W, 32° N). Background is classified as Amazonian knobby plains (Greeley and Guest, 1987). The cluster's superposition and sharp rims, suggest stratigraphically recent origin. (a) MGS/MOC 11-02890. (b) Crater counts suggesting a peak in size distribution at 170 m $\lesssim D \lesssim$ 500 m. The tail of small craters, following an isochron from 16 m $< D <$ 90 m is consistent with the stratigraphic data, suggesting an age possibly $<$100 Myr for this cluster.

and 4b). The loss of small craters in the cluster fits our prediction (Popova et al., 2003) for fragmentation of projectiles and losses of small craters under an atmosphere of $P_S \lesssim$ 300 mbar. The possibility is thus raised that these clusters have something to do with transient, recent atmospheric excursions into higher-pressure regimes. However, it appears unlikely that excursions in P_S could reach such levels. During obliquity cycles the H_2O vapor pressure can change by factors of hundreds, but probably without large changes in P_S (Costard et al., 2001). We believe, therefore, that such high pressures in recent time are unlikely and therefore give low priority to such an explanation.

2.2. Peculiar size distribution of craters in clusters

The crater counts in Figs. 2c, 3b, 4b, 5c, and 6d (not to mention visual inspections) reveal that the crater size distribution in the clusters is unlike any seen among rock fragments, primary craters, or secondary ejecta craters on the Moon, Mars, and other bodies. The usual "primary" or shallow branch of most crater size distributions has a roughly power-law relation (number $N = kD^b$), where k is a constant. Different segments of the distribution have different b values, which equal slopes

in plots of $\log N$ vs. $\log D$ (either in plots using the cumulative number of craters or the incremental number $\log D$ increments, the format used here). For larger primaries, the slope b in a $\log N$ vs. $\log D$ plot is about -1.8, while the slope measured for craters formed from secondary ejecta debris near craters such as Copernicus, as well as the steep branch in the lunar or martian crater "production function" distribution at $D <$ 1 km, is much steeper, about -3 to -3.6 (Hartmann, 1969, 1999). This steep size distribution for secondary ejecta material has been confirmed widely in the Solar System; for example, with a slope of -3.2 (converted to our log-increment or cumulative system of plotting) recently measured on Europa (Bierhaus et al., 2001). All such slopes, or b values, mean that there are *many* more small craters than large ones. In contrast, the diameter distributions in the clusters discussed here are more unimodal, i.e., with a peak at intermediate D. As shown schematically in Fig. 7, we often see a "tail" of smaller craters with a power law, but this is interpreted as representing primary cratering superimposed on the secondary cluster during the time since it formed (plus possible pre-cluster background craters "showing through" between craters of the cluster). The clusters can thus
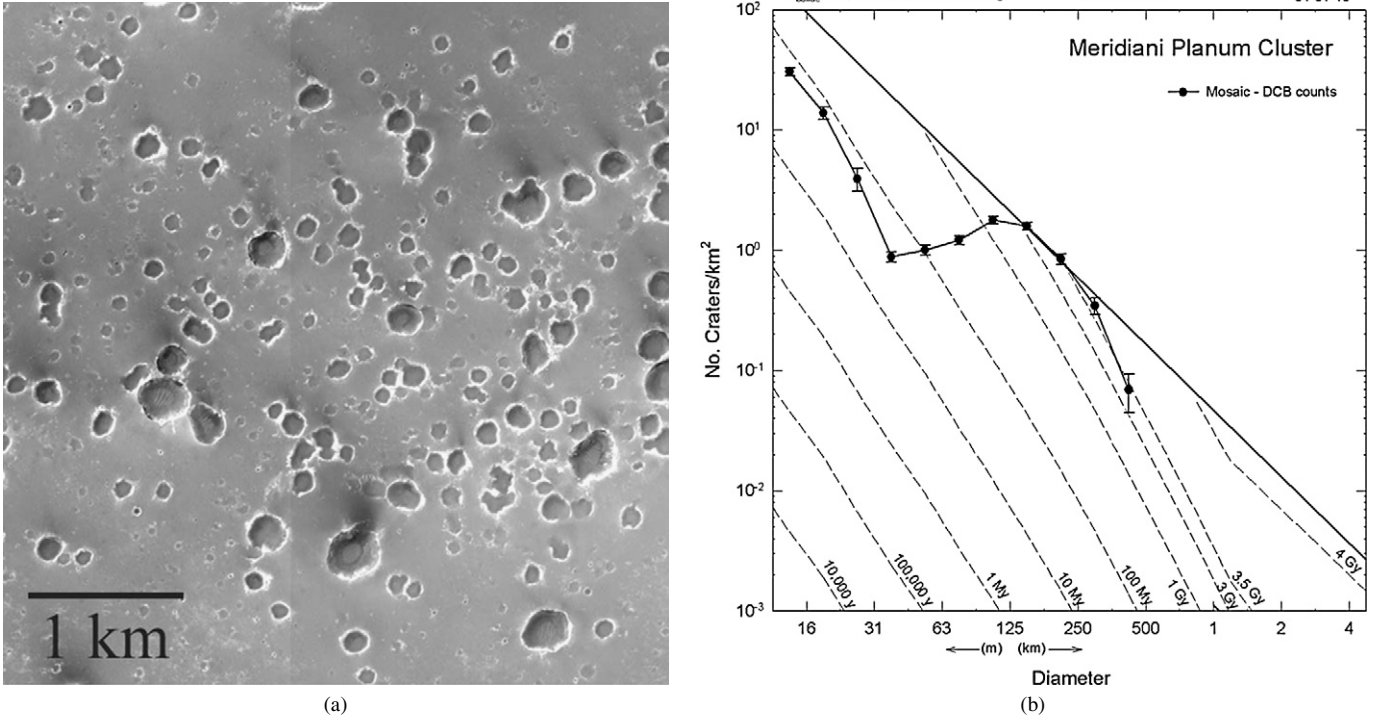
(a)

(b)

Fig. 4. (a) Unusually dispersed cluster in Meridiani Planum (4° W, 2° S). The cluster covers a large area about 60 km across, with somewhat smaller craters than other examples—possibly a product of impact parameters or target conditions at the original crater. Dispersal of craters allows accurate measurement of the total size distribution. Region was classified as a subdued Noachian cratered plateau unit (Scott and Tanaka, 1986), but later work suggests more recent exhumation (Hartmann et al., 2001, Opportunity rover results). (MGS/MOC M04-01900 and other MOC images; mosaic by D.C. Berman, PSI.) (b) Crater counts demonstrating a broad peak in the size distribution at ~50 m $\lesssim D \lesssim$ 250 m. Tail of small craters following an isochron at 11 m < D < 45 m suggests an age <100 Myr for the cluster.

be characterized as clumps of craters primarily in the range of 70 m < D < 900 m, with a peak at around 90 m < D < 250 m. If we assume that these craters came from a normal population of fragments in which only the largest ones were preserved, we would have to assume extreme losses of craters of $D \lesssim$ 70–90 m by some mechanism.

2.3. Constraint on projectile block size

It is important to our discussion that we be able to estimate the size of projectile blocks creating the individual craters in the martian clusters. Using concepts of gravity and strength scaling, as discussed by Ivanov (2001) and Neukum and Ivanov (1994), we can develop an estimate for the ratio of the final crater diameter D to the projectile diameter d. Ivanov (2001) gives the diameter of transition between gravity and strength scaling as being of order 100 m on Mars and 300 m on the Moon. The transition is not well defined and spreads over a range of diameters. McEwen et al. (2005) use the range of 130–260 m; we adopt 200 m. If we assume a density ratio (fragment density/target density) of 1.25, and an impact angle of 60° to the horizontal (see below), we develop equations for the martian ratio of crater size to impactor size, as a function of fragment size and impact velocity V in the strength regime well below the transition diameter [from Ivanov, 2001, unnumbered equation after Eq. (3)] $D/d = 0.139V^{0.55}$. Ivanov's Eq. (3) can be used to develop a more complex equation in the transition zone. For comparison, the following equation may be written for the same parameters in the gravity regime:

$$D/d = 0.882d^{0.22}V^{0.43}.$$

We now examine the crater/fragment size ratio for several velocity regimes. If we consider cosmic impacts at $V = 10$ km/s for a meteoroid of $d_t = 20$ m, we find size ratio values of 30 in the strength regime, ~22 in the transition regime, and 24 in the gravity regime. As will be seen, the same ratio is of great interest for secondary ejecta debris falling back onto Mars. Lorenz (2000) plots impact sites for crater debris and shows that launch at 3 km/s can distribute fragments over much of a hemisphere, and launch at 4 km/s can distribute fragments over most of Mars ($V_{esc} = 5$ km/s). More blocks are produced at the lower launch speeds (Vickery, 1986, 1987). Using launch and fallback velocity $V = 1$–3 km/s for 20-m blocks, we find the size ratio for the three regimes is 8–16, 7–12, and 9–15, respectively.

In the following discussions, when we speak of interplanetary projectile impacts, we will estimate impactor size as ~1/25 of the crater size, but when we speak of secondary fallback debris, we will roughly estimate it as ~1/10 of the crater size.

Fig. 4a shows a cluster in Meridiani Planum (4° W, 2° S) in which craters are unusually dispersed, extending over 30–60 km, allowing easy measurement of individual pits. Fig. 4b gives the diameter distribution showing a range of crater size with a peak at $D \sim 125$ m. Figs. 2c, 3b, and 5c show diameter distributions of other clusters where crater diameters range
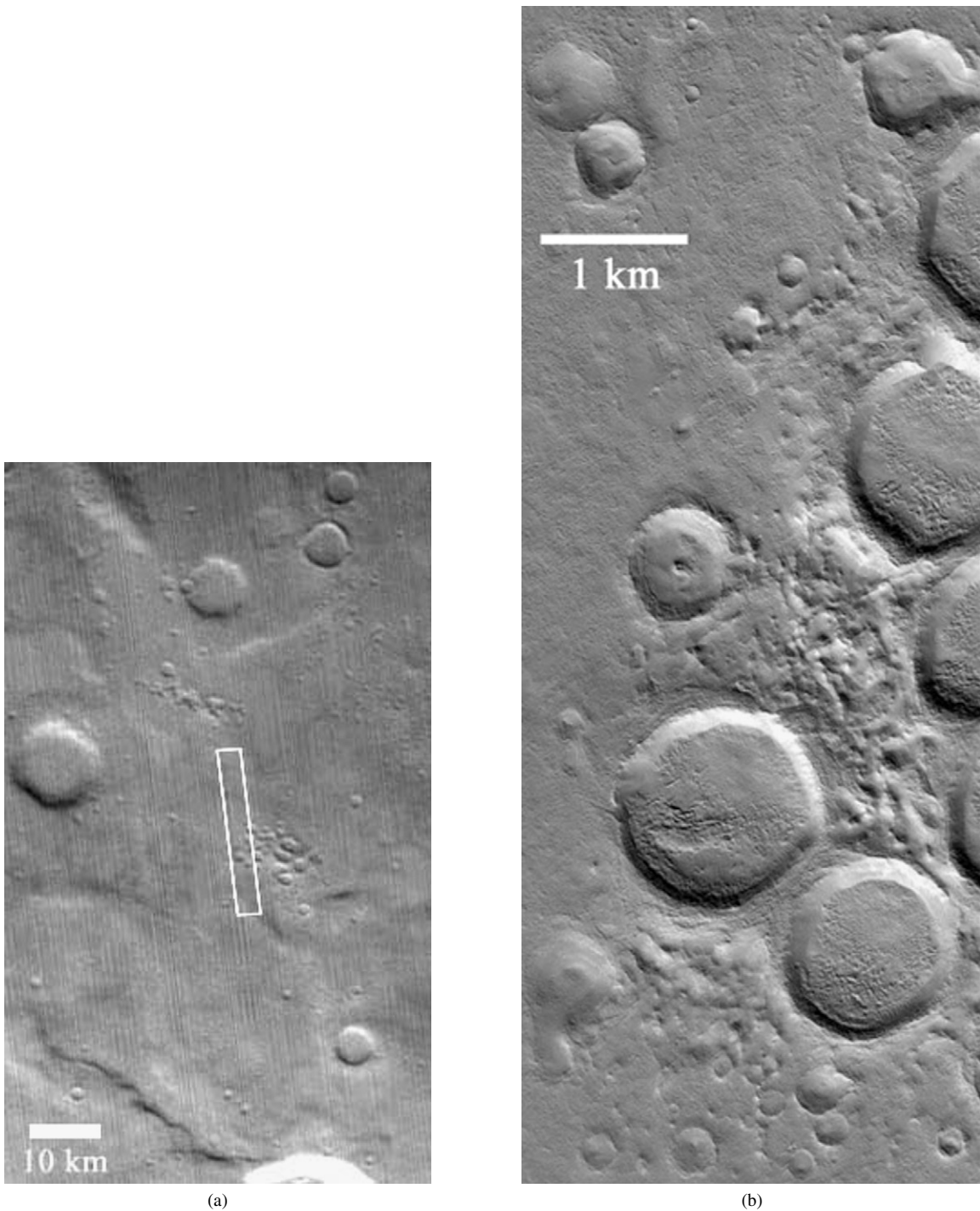
Fig. 5. Two secondary crater swarms, at 316° W, 36° N. These clusters have the highest latitude of our illustrations, in the zone typically affected by mantling processes. They appear to be degraded by mantling processes that have flattened the rims of the larger craters and filled in their interiors. (a) Context frame MGS/MOC M12-01581, showing area of the high-resolution figure. Background is classed as near boundary of Noachian etched and cratered plateau units (Greeley and Guest, 1987). (b) Portion of MGS/MOC M12-01580, showing the pronounced flattening of crater rims. (c) Crater counts show a strong peak in cluster crater sizes at 500 m < D < 2 km. Flattening of curve at 31 m < D < 250 m is interpreted as due to loss of small craters with decameter-scale depths, consistent with decameter-scale depths of mantle deposits. Sparse data on sharp-rimmed craters at the smallest sizes (solid data points) suggest they have formed since the last few high-obliquity (mantle-producing?) episodes, within the last 5–20 Myr.

up to 1 or even 1.5 km (judging a part of the size distribution well above background and usually above even the saturation equilibria level shown by the solid linear curve).

If the impact velocity were cosmic, the impactor diameters d would be roughly 2 to as much as 40–60 m, with severe losses

below $d \sim 2$ to 5 m. If the impact velocity is a sub-orbital value of 3–4 km/s, as in secondary ejecta, d would be more like 5 to as much as 100–150 m, with losses below $d \sim 12$ m and extreme losses below 4 m. The impactors, if they were sub-orbital ejecta blocks, may have been highly fractured or even
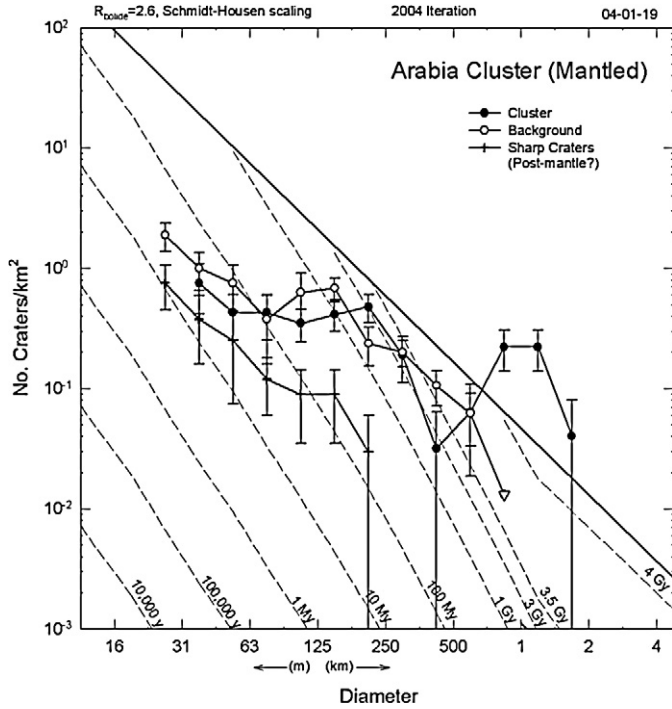
Fig. 5. (*continued*)

dispersing, but they had individual identities as discrete masses of material.

2.4. Constraint on projectile fragmentation and flight time

For normal observed fragmentation events, such as spontaneous comet disruptions, observed meteorite breakups during terrestrial atmospheric flight, or calculated breakup events during atmospheric flight (see Section 3), separation velocities are unlikely to be outside the range of 1 to 100 m/s. Because these clusters have radii of 2000 m to as much as 30,000 m, the time required to produce the separations is likely to be in the order of magnitude range of 20 to 30,000 s (8 h). This suggests that the fragmentation event occurred somewhere in the neighborhood of the martian atmosphere out to Phobos or Deimos, but not much farther.

3. Lateral spreading of meteoroid fragments: theory and observation

One of the first papers to consider the progressive breakup of meteoroids was by Baldwin and Sheaffer (1971). They considered creation of a number of fragments but did not take into account the lateral spreading of fragments. The first estimates concerning interaction of individual fragments were made by Passey and Melosh (1980), who considered forces exerted by interacting bow shocks. They supposed that the velocity u of repulsion for two equal fragments can be described by the relation

$$u = V \sqrt{C * \rho_a / \rho_m}, \qquad (3)$$

where ρ_m, V, are the meteoroid density and velocity, and is the air density at the height of breakup. They analyzed terrestrial crater fields and the constant C was found to be 0.02–1.5.

Note that this model of spreading is relatively insensitive to meteoroid composition and does not take into account any effects of gas production or explosive energy from vapor production. We raise the possibility that a volatile-rich meteoroid, such as an icy, weak cometary body, could dissociate and produce fragments interacting not only with overlapping bow shocks, but also through mutual explosive gas production that could drive them apart. To date, there are no good models of such phenomena. The few observations of weak (carbonaceous, cometary?) meteoroids, relative to iron and stone meteoroids, do not suggest *much* higher explosive, volatile driven spreading in the former, although the fastest fragments may involve such effects in the case of the Benešov bolide, as will be discussed in a moment.

Artemieva and Shuvalov (1996, 2001) considered the interaction of neighboring fragments by direct 3D numerical simulations. The repulsion of two equal fragments, due to gas compression between them through bow shock interaction, is maximized when the fragments are close to each other (enclosed in a single bow shock). It rapidly diminishes as the objects move apart. They determined the constant C for fragments of simple geometric shape. The coefficient C in Eq. (1) is about 0.2 for two equal cubic fragments. In the case of a meteoroid initially disrupted into 13 or 27 cubic fragments with cracks between them (Artemieva and Shuvalov, 2001), the lateral velocity that defines the debris cloud radius can be written in the form Eq. (1) but the coefficient C is higher, ∼1. Artemieva and Shuvalov (2001) considered the evaporation of ordinary chondrite fragments, but it did not substantially change the mechanical forces and coefficient C. For these reasons we assume that even volatile-rich bodies do not fragment with adequate lateral spreading velocity to account for the clusters we see, although this possibility should be revisited in the future.

According to Eq. (1), the lateral velocity, u, is dependent on altitude of breakup. The lateral velocity calculated for fragments produced for entry velocities of 10 and 20 km/s is given in Fig. 8a (solid curve). It assumes $\rho_m \sim 3.5$ g/cm^3 and $C \sim 1$. For entry velocity 10 km/s, we see lateral velocities in the range of 1 m/s (breakup at 50 km height) to 20 m/s (breakup near the surface). If the fragments are not equal, the velocity of the smaller fragment will be higher and fragments' mass (or radius) ratio should be taken into account. Assuming disruption of two pieces (10% and 90% of the total mass) and using relation suggested by Artemieva and Shuvalov (2001), the velocity of the smaller fragment will increase about 1.7 times (dashed curves in Fig. 8), giving lateral velocity 35 m/s for disruption near the surface. All such calculated speeds are far too low to produce the spreading observed in our big clusters.

If the body is cometary, considerably higher initial entry velocities may occur. For entry velocity 20 km/s and an icy density of 1.0 g/cm^3, Fig. 8b shows spreading velocities of fragments from a breakup near the surface as high as 76 m/s for equal-sized fragments and 130 m/s for small fragments. These speeds are closer to those needed to explain the "big clusters,"
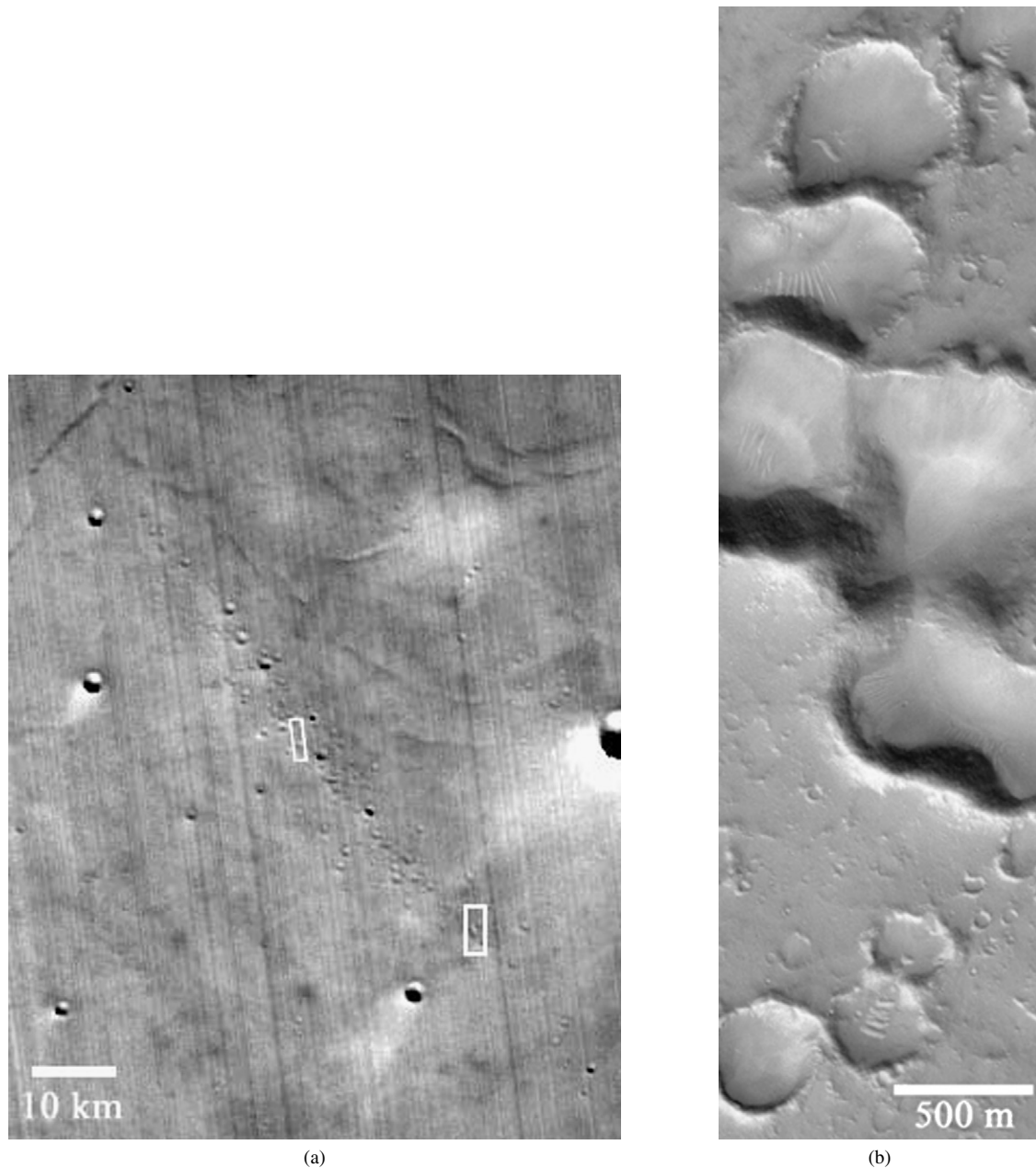
Fig. 6. (a) Secondary craters in the form of a linear array or string, part of a secondary string or ray system (242° W, 27° N). MGS/MOC context frame M12-00958. Background is classified as grooved unit of Hesperian Vastitas Borealis plains (Greeley and Guest, 1987). (b) High-resolution view shows similarity to morphology in crater clusters, supporting the view that clusters are associated with secondary ejecta. MGS/MOC M12-00957. (c) Additional view of a neighboring part of the crater string. Axes of elongated craters are nearly, but not perfectly, aligned with the string axis; they might mark rotational disruption of individual fragments. (d) Crater counts suggest less of a bell shape in the crater (and fragment) size distribution than in other clusters, but do indicate a shallow peak at 100 m $\lesssim D \lesssim$ few hundred m. The less pronounced bell shape may be associated with the craters being part of a ray system, i.e., closer to a primary and having less total flight time than random clusters, and hence less atmospheric drag effects. Open symbols show counts on nearby background surface E and W of the cluster; the interpretation is that the background surface has a model age around 3–3.5 Gyr, but that craters of $D \lesssim 250$ m have suffered losses due to infill.

but again are inadequate to produce the observed cluster widths in the seconds available during post-breakup flight.

Terrestrial observational data relevant to fireball fragments' lateral velocities are very limited. For relatively big meteoroids (meter scale), information is available for five cases, namely the Benešov, Morávka, Peekskill, Spain and Šumava fireballs. The first four fragmented at altitudes 40–25 km. Lateral velocities as high as 300 m/s were recorded for some fragments of the Benešov bolide (Borovička et al., 1998). In the case

of the Morávka breakup, lateral velocity was measured for 27 fragments (Borovička and Kalenda, 2003). Nine fragments had velocities exceeding 100 m/s; the number of fragments with velocity near zero is underestimated because numerous fragments following nearly the same trajectory could not be measured individually. For Morávka, a lateral velocity of 300 m/s was found for the fastest fragments, and velocities about 50 m/s were more typical (Borovička and Kalenda, 2003). It is estimated that only 10% of fragments had velocity exceeding
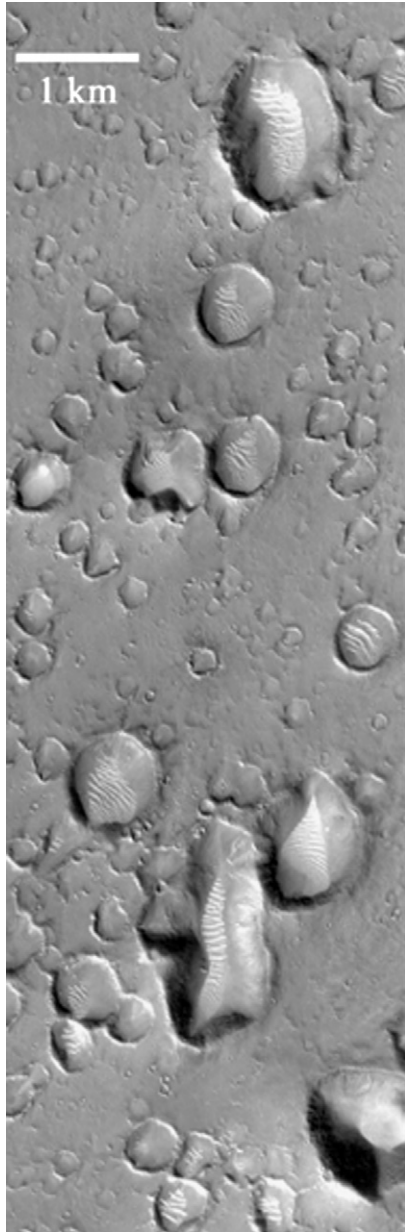
(c)
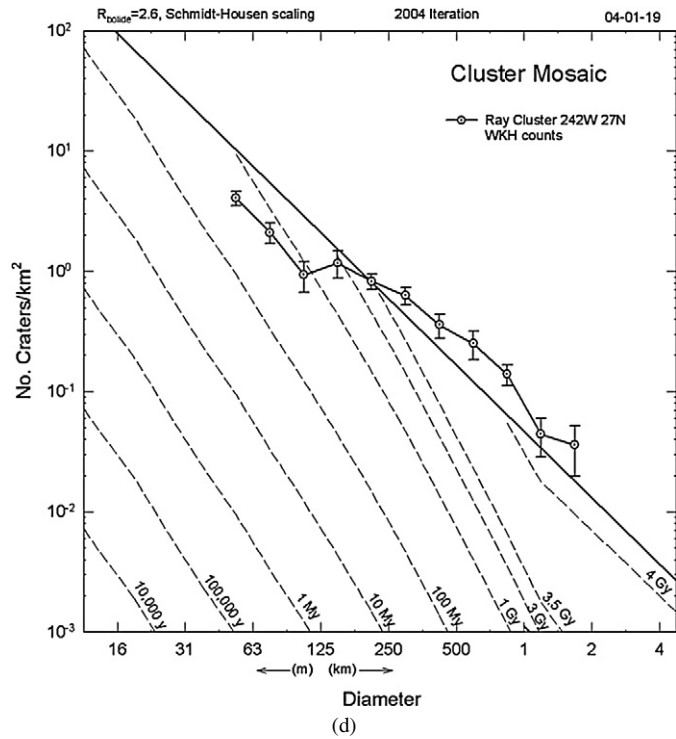
(d)

Fig. 6. (*continued*)

100 m/s (Borovička et al., 2001). The Peekskill fragments had velocities of the order of 60 m/s. Lateral velocities of some fragments of about 50–200 m/s are likely in the case of the Spanish bolide (Docobo and Ceplecha, 1999). In all cases fragments were estimated to be several or several dozens of kg in mass.

We now compare the theoretical and observational estimates of the lateral velocities for Benešov and Morávka, the best-observed cases. Observed fragmentation occurred at about 30–40 km altitude for these two. The atmosphere density at these altitudes is comparable with the density of the martian atmosphere at about 0–15 km altitude. The entry velocity of Benešov and Morávka was about 20 km/s. The theory predicts lateral velocities for the major part of fragments to be in the range of about 29–93 m/s for Benešov (fragmentation al-

titude $H_{\mathrm{fr}} \sim 40$–30 km, $\rho_m \sim 2$ g/cm^3) and about 40–69 m/s for Morávka ($H_{\mathrm{fr}} \sim 30$ km, $\rho_m \sim 3.5$ g/cm^3), as seen in Fig. 8. This agrees reasonably with the observations, but the highest observed velocities appear to reach somewhat higher values than predicted, suggesting additional forces accelerating bodies laterally, as also noted by Borovička and Kalenda (2003), who noted maximum lateral speeds "an order of magnitude more than can be explained by aerodynamic loading."

At a more detailed level, the Benešov bolide is the only bolide for which complete data including light curve, spectra, and trajectory are available and specific modeling is possible. Its behavior was well reproduced by the progressive fragmentation model (Borovička et al., 1998). The best estimate of the initial mass is 3000–4000 kg with a density of 2 g/cm^3. The separation angles of Benešov bolide fragments were compared
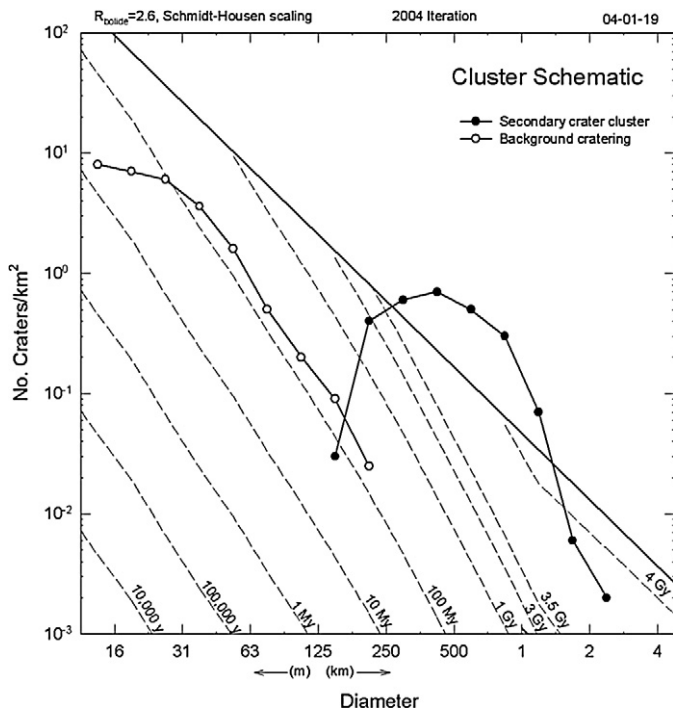
Fig. 7. Schematic interpretation of crater diameter distributions observed in large martian crater clusters. The bump, or bell-curve-like distribution in the cluster (not observed on normal martian surfaces), is interpreted as the size distribution of the impacting secondary fragments, with losses of small fragments due to atmospheric interactions. The power-law tail of small craters is interpreted as craters superimposed on the cluster by normal primary cratering.

with theoretical predictions according to Eq. (1) (Borovička et al., 1998). At low altitudes (25 km) the predicted spreading angles and velocities of fragments are in agreement with observations. For three fragments at higher altitude (around 30 km), the observed angles are of the order of magnitude as theoretical ones, whereas for two other fragments they are bigger by several times. Borovička et al. (1998) proposed that this deviation was caused by peculiar aerodynamic shapes among certain fragments. High altitude fragmentation was assumed in the cases of Benesov and Morávka bolides, although the resulting fragments were not directly observed because they could not be optically separated from the main mass due to low lateral velocity at these altitudes (50–60 km), in agreement with our theoretical estimates. In a similar vein, Nemtchinov and Popova (1997) successfully used the same lateral velocity theory to describe the Sikhote-Alin crater field.

To summarize, the existing theoretical approach suggests there are no classes of meteoroidal bodies that would fragment during entry in a way to produce the observed big martian crater clusters. We may use the progressive fragmentation model with lateral velocity according to Eq. (1), and $C \sim 1$ to estimate lateral velocities. Extreme observed values may be higher than predicted by the somewhat idealized theory, depending on forces of repulsion and relative momentum among the fragments, as suggested also by Artemieva and Shuvalov (2001) and Borovička et al. (1998). Lateral spreading of fragments causes formation of strewn fields of meteorites and craters in the case of atmospheric disruption. If the meteoroid is strong and sur-

vives the first part of atmospheric passage to be disrupted at low heights, its fragments may have a large lateral velocity but only a small time for flight, and they will be not as widely strewn as our observed martian clusters. Conversely, if it is disrupted at high altitude, the predicted lateral velocity is small and again the separation is inadequate. We conclude that lateral spreading after fragmentation *of incoming meteoroids* can explain only the "small crater clusters" with widths of hundreds of meters, but not "big crater clusters," extending over 10 km, or even >20 km.

After a fragmentation event, the resulting strewn field of meteorites and/or craters is dependent on details of the fragmentation process. We still have some uncertainties here. There are several approaches to formation and numbers of fragments in the breakup event. Artemieva and Shuvalov (2001) assumed the production of equal-sized pieces. Hartmann (1969), however, showed that known terrestrial and planetary fragmentation events produce not equal-sized pieces, but approximately power-law distributions with many more small pieces than large ones. Such a power law of fragment size distribution was assumed by Nemtchinov and Popova (1997) and Borovička et al. (1998) in modeling of Sikhote Alin and Benešov. In a somewhat different approach, Artemieva and Shuvalov (2001) assumed successive breakups into fragment pairs with randomly chosen size ratios. We have compared the last two approaches, which led to somewhat different mass–frequency distributions of final fragments. The model with disruption into fragment pairs shifts the size distribution to bigger fragments and slightly increases the energy fraction released on the ground, but the difference is not essential. Maximal crater size and size of the scattering ellipse of crater clusters from incoming meteoroids are similar under both fragmentation models. All these assumptions suffer from limitations. The random choice of two fragments in every breakup does not produce the numerous small fragments observed in most real events. Power-law size distributions provide better matches to nature, but need more work in specifying maximal fragment size under different disruptions conditions.

3.1. Formation of "small crater clusters"

In Popova et al. (2003) we used two different models to discuss meteoroid fragmentation: the liquid-like (or "pancake") model, in which the meteoroid breaks into fragments treated as a swarm traveling as a single mass, and the progressive fragmentation model, in which each initial fragment may undergo later breakup as stresses increase in the lower atmosphere. An important observation is that numbers of meteoroids have been seen to break up at low stress in the very high atmosphere, implying a low strength and hence a highly fractured initial state while traveling in space, even though the final fragments have the higher strengths of coherent rock. We infer that the parent meteoroid masses in these cases are highly fractured during asteroid collisions, but break up into individual meteorite specimens of higher strength because the fractured parent mass breaks into sub-units of coherent rock. In nature, large objects of a given material are typically weaker than smaller sub-units of the same object, because of included fractures and imper-
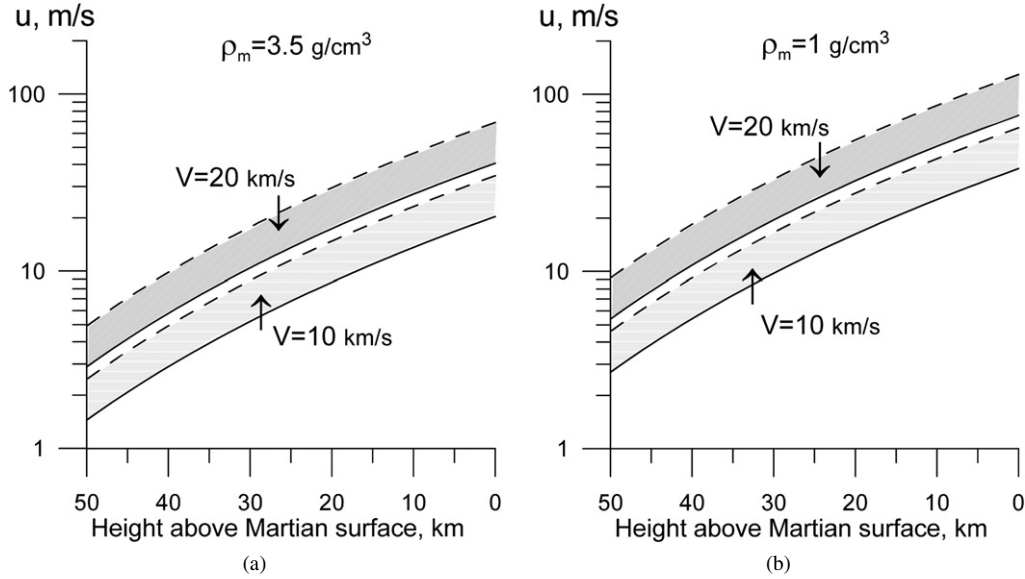
Fig. 8. Estimation of spreading velocities for pieces of a fragmented meteoroid, as a function of height of fragmentation event in present martian atmosphere, according to Eq. (1). Two densities are given to bracket likely cases: (a) 3.5 g/cm³ for dense stone, and (b) 1.0 g/cm³ for an icy cometary body. Solid line gives case for two equal-sized fragments, and dashed line for the smallest pieces in a size distribution. Entry velocities of 10 and 20 km/s are shown. Spreading velocity increases with air pressure, which means that the highest values are for breakup events near the ground. The values are consistent with our small cluster sizes, but even the highest values, for a high velocity icy body (b, upper right), are not adequate to produce our large clusters during the flight time of an incoming meteoroid.

fections; this is particularly true in a collisional fragmentation regime such as experienced by asteroids.

Only a single crater is formed in the liquid-like model, by definition, whereas the progressive fragmentation model allows multiple craters. In Popova et al. (2003) we used a strength scaling law or strength data from observations together with the progressive fragmentation model and found that numerous craters are really formed in the case of separated fragments. These craters may overlap and form a single visible crater if the spreading is small enough; otherwise a crater field is formed with partially overlapping or separate craters. We estimated the effective strength as

$$\sigma = \sigma_s (m_s/m)^\alpha, \tag{4}$$

where σ and m are the effective strength and mass of the larger body and σ_s and m_s are those of a tested specimen; α is a scale factor.

In the current martian atmosphere a fraction of the strong meteoroids ($\alpha = 0.25$ in strength scaling law), with typical entry velocity about 10 km/s, and projectile diameter $D_p < 10$ m (in the range of model applicability), are disrupted at relatively low altitudes and have no time to form a large strewn field. We consider here the average entry angle of 45°. Fragments are not too numerous and craters with maximal size about 20–50 m are produced, but tend to overlap. Even a single crater may be formed, similar to the one found in the liquid-like model, although its shape may be more irregular. Since both models produce a similar result in the case of strong chondritic bodies, we conclude that the precise mode of disruption will not be essential in determining the total crater size frequency distribution among the impact craters.

However, in the case of weaker bodies (for example, chondrites with $\alpha = 0.5$ in strength scaling law), disruption starts

higher above the surface, and more numerous separate fragments appear. Resulting craters (with maximal size about 5–10 m) are separated enough for a strewn field of craters to form. The precise separation of craters depends on details of fragmentation and fragments' motion. The predicted distance between craters and degree of overlap also depend on crater size estimates (i.e., scaling laws used to estimate crater size).

In a hypothetical denser past martian atmosphere (with surface pressure up to 100 mbar), even the strong chondritic bodies will cause formation of strewn fields of craters, whereas weaker ones can be so severely fragmented that they will not produce hypervelocity craters at all. In very dense atmospheres (300–1000 mbar), progressive fragmentation leads to disappearance of hypervelocity impact craters due to formation of numerous small fragments with low terminal velocities.

The Benešov bolide, mentioned above, offers a good example of these phenomena. It was successfully described by Borovička et al. (1998), and its behavior seems typical for meter-sized bodies. There is direct observational evidence of Benešov's fragmentation at altitudes of 38–31 km and of catastrophic disruption at 24 km. The crucial point is that the bolide was significantly decelerated already at the altitudes between 50 and 40 km, and enormous luminosity was produced below 40 km. It was therefore concluded that the meteoroid must have been fragmented already at an altitude of 60–50 km. After the high altitude breakup, further fragmentation events certainly followed. Benešov thus fits the progressive fragmentation model, and we can adapt this entry description to Mars, changing primarily the atmospheric parameters.

If a similar body (initial mass 3000 kg, initial velocity 21 km/s, 9° to vertical) enters the martian atmosphere, according to our model it reaches the surface as a swarm of fragments after two breakup events (35 km, apparent strength 2.3 bar;
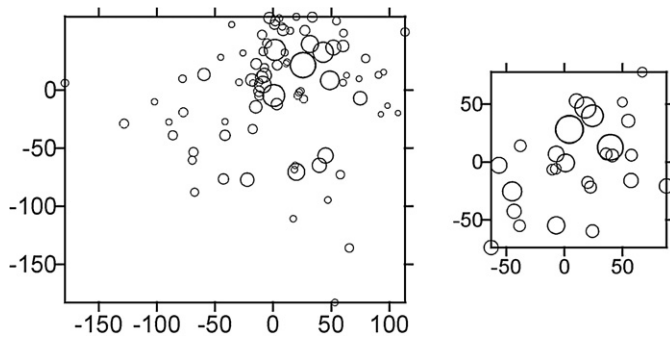
Fig. 9. Simulation of small cluster of craters, based on progressive fragmentation model with lateral spreading of fragments. Crater fields are formed after fragmentation of 1–1.5-m meteoroids with apparent strength of about 1–10 bar, entering the martian atmosphere with velocity about 10 km/s.

19 km, apparent strength 23 bar) and forms a crater field about 200 m in size. In a hypothetical denser atmosphere, somewhat larger crater fields would be formed. The size of the strewn field will increase with atmospheric density, whereas crater sizes will decrease and disappear above ∼300 mb surface pressure. In the current atmosphere, a similar body with entry velocity 10 km/s, more typical for Mars, will experience one disruption and form a crater field about 100 m across.

Calculated appearances of "small crater clusters," formed after fragmentation of 1–1.5-m meteoroids with apparent strength about 1–10 bar, are shown in Fig. 9. Precise numbers of craters, their sizes and displacement are dependent on assumptions used, but we can reproduce the general properties of small craters clusters using reasonable values of parameters. We thus affirm our suggestion in Popova et al. (2003) that the "small crater clusters" we have described on Mars are due to breakup of typical stony meteoroids in a martian atmosphere, essentially matching that of the present-day planet.

3.2. Volatile rich bodies: rapid spreading?

Because of the possibility that volatiles play a role in dispersing fragments and producing crater clusters, we are especially interested in the observed behavior of volatile-rich meteoroids. The only detailed observed case of such a body (or at least a meteoroid with cometary characteristics) is the bolide Šumava. It was one of the brightest bolides detected by the European Network (Borovička and Spurný, 1996). At high altitudes, 75 to 59 km, its light curve showed four major maxima. Disruption events are needed to explain the light curve and deceleration. No fragmentation in the sense of visible fragments was detected but the luminous image on photographs was produced by a source of considerable elongation, probably a string of fragments. Assuming the flares on the light curve are associated with breakups, the fragmentation pressure was unusually low, about 0.25–1.4 bars. The extreme fragility of Šumava supports its cometary origin.

A radiative radius, i.e., the effective radius of a body or of a cloud of fragments and vapor causing the same luminosity as observed, was estimated by Nemtchinov et al. (1997a). The radiative radius of the bolide increases during flares, and the

velocity of lateral expansion in the first flare appears to be 50–60 m/s. The value is larger than the lateral velocity u which could be caused by simple aerodynamic loading, based on our Eq. (1).

Aerodynamic loading alone thus cannot explain the great rate of meteoroid expansion and great effective radius of the falling body. To explain the observation, Borovička and Spurný (1996) supposed that the first flash resulted from a sudden mass loss of 400 kg due to fragmentation. The word "sudden" implies a time interval of about 0.1 s or a distance along trajectory of about 2–3 km. Their model gives a reconstruction of the bolide radiation, but a simple destruction (loss of strength) could not give a great energy release and a radiation flash, as was demonstrated in the simulations of Shoemaker–Levy 9 comet fragment deceleration and ablation (Nemtchinov et al., 1997b; Shuvalov et al., 1997). Thus the fragmentation (which leads to high energy flashes) should involve not only mass loss and destruction, but also a mechanism of expansion which is necessary to diminish the density (and cause deceleration). One of the possible mechanisms may be a volumetric evaporation, in which bubbles of vapor appear within the near-surface layer, not just at the surface, resulting in explosion-type expansion. These findings support our earlier suggestion that improved modeling of entry physics for volatile-rich meteoroids is urgently needed.

Nemtchinov et al. (1999) proposed a hypothesis of Šumava-like meteoroid fragmentation during atmospheric entry. According to current models (cf. Dessler, 1991), a comet is a low density (0.1 g/cm^3), dirty snowball covered by an insulating layer (crust) with a depleted amount of volatiles and thickness of about 1–4 cm. The lowest value of strength was estimated as about 5×10^3 dyne/cm^2. The aerodynamical loading is higher than this limit by an order of magnitude at altitude of about 80 km. Under the action of aerodynamic forces, the porous body will disrupt and/or distort, so that the shape of the entering mass briefly becomes similar to a flattened disk (cf. next section).

Whatever its detailed structure, the disk will fragment, with fragment size modeled as comparable with disk thickness. The smallest fragments will evaporate more rapidly than the larger parent meteoroid. Due to aerodynamic loading and/or partial evaporation of the volatiles at 80 km altitude above Earth (corresponding to about 50 km above Mars), the fragments and/or small volumes of the vapor spread laterally. The cloud of vapor and fragments acts as a gaseous meteoroid with an increasing cross-section. The initial velocity of expansion is probably higher than that caused by simple aerodynamic loading, as noted above.

We have considered the evaporation and motion of the thin disk of vapor and small fragments under the influence of radiation in a model with 1D cylindrical geometry (Popova et al., 1999). It was assumed that the small-sized fragments and intervening vapor move together. This model indicated that such a cloud of fragments plus vapor can expand with higher spreading velocities than aerodynamical ones in relatively thin atmosphere.

Volume evaporation of the initially formed fragments permits us to obtain a high value of lateral expansion velocity (up

to 100–300 m/s), although this effect should be verified by 2D modeling. Additionally, only small fragments (0.1–10 cm in size) were considered and there is no foundation to suggest that it is valid for fragments, meters or tens of meters across. Nonetheless, as seen in Section 2.3, the projectiles we are dealing with are as small as 2 to 50 m in diameter, and in the event of some sort of steam blast explosion from a volatile body (not well represented in present theory), it is plausible that at least the smaller bodies could be accelerated to higher lateral speeds than described in current models.

To summarize the arguments so far, the existing models and observations are consistent with weak meteoroids breaking up in the martian atmosphere and spreading at lateral velocities of tens of m/s, causing the observed "small clusters" of 10–20 m scale craters spread over 100–300 m. Theoretical models give some suggestion that weak cometary bodies could break up and produce small fragments spreading at higher velocities exceeding 100 m/s. These might produce some of the most dispersed "small clusters." However, the present models fail to produce conditions that would explain our "large clusters" of 500 m craters spread over 5–30 km. Furthermore, we see no smooth continuum between the small and large clusters; they seem to represent two distinct phenomena. Therefore we now seek other explanations of the "large clusters."

4. Comet breakup as a source of "large clusters"

An early response to the clusters was to suspect that they might represent the impact signature of a hitherto unknown class of weak cometary bodies that might explode into fragments upon entering the martian atmosphere (Hartmann and Engel, 1994). This possibility seems especially attractive in view of the rubble pile or cometesimal model. The idealized rubble pile comet as envisioned by Weidenschilling et al. (1997) could be made of 100-m spheroids of dusty ice, held together with near-zero tensile strength. The strength pressure of each icy spheroid might be 1–2 bar, but it could separate with much less stress as the incoming body flattens during atmospheric passage. Volatiles might drive them apart at high lateral velocities. This hypothesis would explain the unusual size distribution we observe among the crater clusters, because such a comet would create a swarm of hectometer-scale craters.

In this case, the large martian crater clusters would constitute direct detection of a weak, volatile-rich class of impactors hitherto undetected on Earth, and it would become a test of the Weidenschilling comet model. Attracted by the idea of crater clusters as signatures of a new phenomenon, we considered several possible scenarios of comet breakup.

4.1. Comet breakup in the martian atmosphere

The initial hypothesis was that a weak rubble pile explodes during passage through the martian atmosphere. As described above, the fatal problem is that the 2- to 18-m scale constituent building blocks (cf. Section 2.3) have only a few seconds to spread laterally by 5 km or even several times more. As presented in Section 3, we find no plausible way that such large

fragments could be accelerated to the several km/s speeds necessary in the time available, although we caution again that existing models may not deal adequately with explosive disruption of volatile rich bodies. The presence of highly volatile ices in comets and the absence of a complete theory about explosive gas effects means that this hypothesis should be left open for future work, especially since it explains the observed size distribution of crater clusters; but the present base of knowledge, and the absence of any detection of high velocities in observed carbonaceous meteoroid fragments, leads us to give low probability to this model.

4.2. Comet breakup at a distance in space

We considered the breakup of rubble pile comets in space due to collisions or spontaneous breakup, as has been observed among various comets. However, as argued in Section 2, the breakup must occur within a few hours of Mars. Such breakups by collision or spontaneous comet phenomena are unlikely to occur in adequate numbers, and we reject this idea.

4.3. Comet breakup by tidal forces

An additional possibility, to preserve the rubble pile comet size distribution but still have separation of fragments, is tidal breakup of weak comets. If a very near-zero tensile strength rubble pile comet approaches Mars, it could be slightly disrupted already as it passes inside Roche's limit, before it hits the atmosphere. At 20 km/s, if Roche's limit is about 7000 km out from Mars, we have about 350 s for the icy spheres to desegregate into a swarm of separate bodies. We would need dissociation speeds preferably above 10 cm/s to get them substantially apart—this would produce a cloud of 100 m icy spheres >35 m apart.

One of us (D.C.R.) ran a model to examine these issues in a simple way. We took a 35-body rubble-pile comet, with individual bodies having diameter 400 m and the comet having diameter 1400 m and bulk density 1 g/cm^3. This "comet" moves radially toward Mars. The model measured the maximum particle separation from the center of mass of the pile (i.e., maximum radius) as a function of time. The rubble pile started 10,000 km from the center of Mars, moving at 10 km/s. This puts it roughly two Roche radii out initially. Fig. 10 shows the maximum separation as a function of time—it increases just over 735 m, so that some disruption occurs, but not enough to separate the bodies to the degree needed to explain the clusters. The dissociation speeds are only on the order of 0.03 m/s. In Fig. 10a, the "bumps" in the curve are due to the fact that we started with an unequilibrated rubble pile which is still in the process of settling down when it starts getting stretched apart. We note that the stretching in this case is mainly along the line of flight, so that its effect on separating the impact positions and increasing cluster size is minimal. We conclude that the tidal stretching alone is not likely to be adequate to explain the observed clusters.

Another idea was proposed by Weidenschilling (private communication) to help get further separation of fragments be-
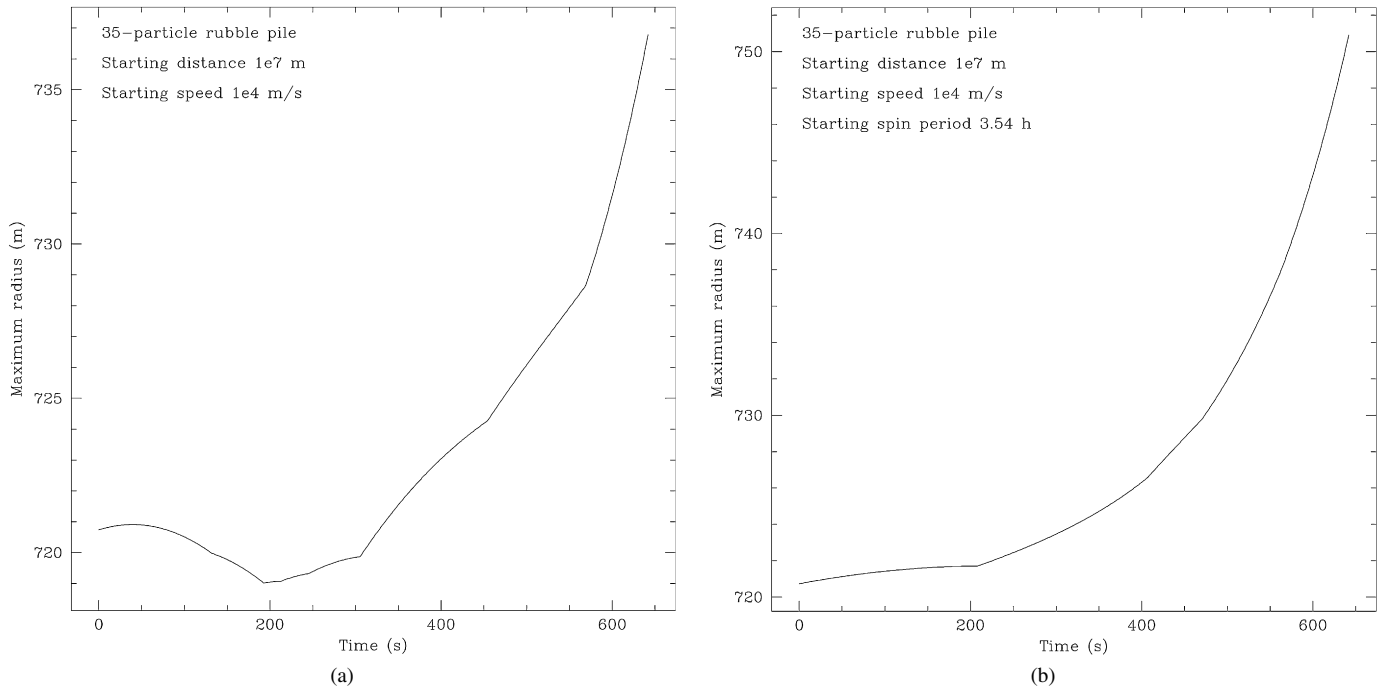
Fig. 10. Calculated spreading of a comet nucleus approaching inside the Roche limit of Mars. The comet has 720 m radius, composed of 35 pieces held together by gravity. (a) Non-rotating case, spreading by only 15 m or 2% before hitting Mars. (b) Case of rotation approaching instability, resulting in spreading by 30 m or 4%. See text for further discussion.

fore hitting the martian atmosphere: rotation. If the comet is already near limits of rotational stability, do the tidal forces help spread it out before it hits the atmosphere? A plot for the same comet spinning close to its breakup limit (3.53 h) is presented in Fig. 10b. The assumed rotation roughly doubled the dispersal and would help spread the constituent bodies laterally to the line of flight. However, the net effect, while interesting, seems inadequate to allow comets to explain the observed "large crater clusters." Our results agree with earlier consideration by Bottke and Melosh (1996) who found that only a small fraction of rubble pile asteroids that encounters Mars become separated at enough large distances to produce a double crater.

The remaining caveat for future research might be that if a rotating Weidenschilling-type comet disperses into a swarm of 100-m scale bodies a few meters apart from each other before hitting the atmosphere, the inadequately-modeled effects of gas production, interparticle pressure buildup, and interacting shock waves could produce lateral explosive motions that have not yet been adequately modeled.

5. Phobos and Deimos as sources of "large crater clusters"

In this hypothesis, clusters form as a result of fragments knocked off Phobos or Deimos by impacts. Impacts are most likely on the side facing away from Mars, especially on Phobos, where a large solid angle of the sky is blocked by Mars. We consider several processes.

First we consider spallation of fragments off the Mars-facing side from impacts on the far side. The escape velocity for Phobos is 11 m/s. Ivanov (1991) and Asphaug and Melosh (1993) have shown that even for the very large impactor creating Stickney crater (energy about 100 Mt for a 100-m radius impactor),

the velocity at the Mars-facing antipodal point is insufficient to overcome gravity (velocity of particles is only about 1 m/s, i.e., less than the escape velocity by a factor of about 10). Deimos' radius is smaller by a factor of two than that of Phobos and its escape velocity is only 6 m/s. Nevertheless, the impactor required to produce spallation fragments moving faster than the escape velocity from this satellite should be rather large and such an impact is a very rare event.

Next we consider secondary ejecta fragments directly from craters on Phobos and Deimos. At the radius of 23,000 km or $7R_{Mars}$, the orbital velocity of Deimos is 1.2 km/s. To cancel this velocity and provide vertical descent, we may produce ejection from the side opposite to the rotation direction, i.e., at the trailing side. If we completely cancel the orbital velocity, all the fragments will fall vertically due to gravity, almost with the free fall velocity. Alternatively, if we increase the velocity of some fragments by about 960 m/s for Phobos and 500 m/s for Deimos, the fragments will leave the martian gravity field. Thus, the trajectory of fragments strongly depends on their ejection velocity, the angle of impact, and the angle between direction tangential to the surface at the point of impact and the orbit. The ejecta curtain is a very wide cone and fragments fly with velocities within a wide range; only a small part of the fragments will fall onto Mars. Only a small fraction of ejecta from the small number of impacts on Phobos and Deimos produce clusters, and the impacts must produce multi-km-scale craters in order to produce the necessary numbers of 10- to 50-m scale ejecta blocks. The observed clusters would appear to come from multiple primary impacts, since they probably have different ages (see the crater count diagrams) and the satellites probably do not have enough young craters. In summary, im-

pacts on Phobos and Deimos seem unlikely to be a source of the numerous crater clusters treated here.

6. Secondary ejecta as the source of "large crater clusters"

The above considerations drive us to the hypothesis that the clusters are produced by secondary ejecta. In support of this, clumps of secondary craters in known strings of secondary ejecta craters resemble our isolated crater clusters (compare Figs. 5 and 6 with Figs. 2, 3, and 4). The basic idea here is that because the clusters are far from primaries, they represent large blocks of ejecta that fragmented not just during the few seconds of *descent*, but during launch and *ascent* through the atmosphere, followed by lateral spreading during many minutes of flight in space, and then followed by descent through the atmosphere. In other words, in terms of a theoretical model, the initial process represents an "upside down" entry problem.

This model *explains the absence of isolated clusters on the Moon* in spite of their frequency on Mars: once launched, weak lunar secondary blocks, in the absence of atmosphere, are not dissociated on ascent or descent, whereas the martian blocks are. The ejected lunar block makes a single crater (hard to distinguish from a primary); the ejected martian block, if launched to a large distance from the primary, dissociates in the atmosphere and makes a cluster. In this model, as discussed in Section 2.3 on scaling laws, the inferred diameter of the fragment is $d \cong 1/10$ of the crater diameter.

There are several important issues in this hypothesis, including the question of whether primary impact craters can launch large enough blocks, and whether these blocks can break up to produce the observed size distribution.

6.1. Clusters and primary craters

The clusters that initiated this investigation are relatively isolated from other craters, as noted above. In most cases, the parent primary is not obvious, and we explain this by the long flight times needed to dissociated the fragments involved. In a few other cases, similar clusters do appear to be part of secondary crater swarms. Fig. 6a shows a linear swarm of secondaries roughly radial to, and possibly associated with, a fresh looking crater of $D = 33$ km at 27° N and 242° W. Figs. 6b and 6c show that the crater groupings within this association appear very similar at high resolution to the other clusters. The pair of clusters in Fig. 5a may also represent a transitional example of a poorly defined ray-like string of secondaries, perhaps near the maximum distance for coherent "rays."

However, we will now hypothesize that each cluster is associated with a discrete ascending parent block that is highly weakened and/or fragmented during the primary impact and ejection process, causing it to fall apart into pieces that dissociate during ascent through the atmosphere. In this scenario, the atmospheric breakup allows the swarm of fragments to spread to the observed widths of clusters during sub-orbital flight, before they reenter the atmosphere, so that they impact in a cluster with the observed dimensions.

We now ask whether single craters could launch single blocks big enough to contain all the material in a cluster. Starting from Fig. 2c, imagine a somewhat extreme example of a cluster the equivalent of 125 craters, each 250 m in diameter. This means we need a block made up of 125, 25-m pieces, which could thus be a cube 5×25 m $= 125$ m on a side. Even if we attach a few additional 100–150 m pieces to allow for the largest craters in the cluster, we can explain the clusters by the material within a parent block ∼300–400 m on a side. In a more detailed test, we counted the total visible craters in the cluster of Fig. 2a, estimated projectile diameter $d = D/10$ (per Section 2.3), and summed the total volume of projectiles. Most of the volume is in the mid- to largest-size craters. This gave a spheroidal parent projectile with diameter ∼340 m, which must break into smaller pieces during ascent.

As noted in Section 2.3, our figures show that the largest discrete fragments making craters within the clusters, for suborbital ejecta, just reach diameters up to 100–150 m across. Is this plausible? Surrounding the 226-km martian primary Crater Lyot, Vickery (1986, 1987) identified secondary craters which she listed as formed by ejected blocks ranging up to 3 km diameter, indicating that sufficiently large craters can easily launch the necessary hectometer-scale, quasi-coherent blocks. We note, however, a mass-velocity inverse correlation such that blocks thrown to very large distances from Lyon would have $d < 3$ km. To summarize, we conclude that a sufficiently large crater can launch discrete, though fractured, blocks of adequate size.

6.2. Creating the cluster size distribution

As noted in Section 2.2, clusters are closely spaced craters with similar sizes, and their size distribution is uncharacteristic of the normal, roughly power-law size distribution of debris. We now look for ways to alter the normal power-law fragment size distribution among ejected fragments into the observed distribution. As noted in Section 2.3, we observe deficiencies (relative to normal secondary crater size distributions) of craters in the range 45 m $< D <$ 125 m, implying losses of secondary debris with diameters d around 4 to 12 m, with additional losses at d as much as 50 m, depending on the cluster. Severe losses are implied below $d \sim 2$ to 12 m.

One modest loss mechanism might involve overlap among cluster craters. As a thought experiment, if one imagines a "randomized" set of small fragments and one much larger fragment, all hitting the same spot, one sees that the first small impacts would be mostly wiped out by the large one, and then only the final small impacts would be recorded—thus reducing the record of small objects relative to their initial numbers. The effect is stronger if small bodies are mixed among a string of large bodies. This effect may play some role in tight clusters, but the strong bell-curve shape in the Meridiani Planum cluster (Fig. 4c), where the craters are widely separated and have very little overlap, shows that this is not a full explanation.

A second, more likely mechanism is separation of small bodies from the swarm by atmospheric drag. On Earth, this effect is well known. In terrestrial strewn fields, large bodies
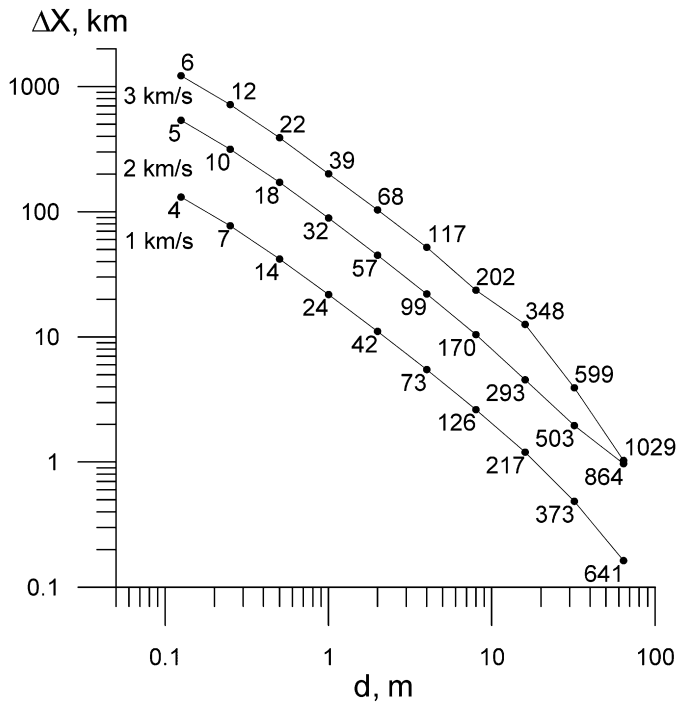
Fig. 11. Drag effects for a swarm of secondary ejecta particles launched from a crater at 1 km/s (lower curve), 2 km/s (middle), and 3 km/s (upper curve). Abscissa shows projectile diameter, labeled d, in meters. Ordinate shows lag distance, caused by drag, for particles of different mass, relative to a very massive particle with no drag. Numbers along the curve show diameter of secondary craters (meters; scaled to projectile sizes and impact velocity). See text for discussion.

impact at the leading end of a swarm, but with a trail of small fragments dragged out behind them during descent to form an elliptical swarm (Frost, 1969; Passey and Melosh, 1980). On Mars, swarms of secondaries *near* primary craters show the usual steep power-law size distribution of lunar secondaries, not the bell-shaped distribution we find in isolated clusters— which supports the idea that the sorting happens only during longer flights with more atmospheric interaction and more time for separation of swarm members.

In the current martian atmosphere drag can indeed affect bodies smaller than some meters or tens of meters. We have made sample calculations of these drag effects as shown in Fig. 11, which shows conditions for secondary bodies with diameters given on the abscissa, launched at 45° from a crater at three test velocities, 1 to 3 km/s. The ordinate gives the lag distance Y for the separation of the smaller fragments from the main cluster of large ones. The figure shows that for launch velocities of 3 km/s, bodies smaller than 5 m, causing craters smaller than about 125 m, would land 30 km or more from the largest projectiles (i.e., the main cluster of large craters); the still smaller bodies causing craters smaller than about 60 m would land more than 100 km away. Craters with $D \sim 200$–350 m would land as much as 10 km from each other. For 2 km/s velocity craters, $D \sim 170$–900 m (projectile sizes $d \sim 7$–70 m) would be spread along a 10-km segment. This suggests that drag effects are the right order of magnitude to cause at least part of the ob-

served loss of small craters from the clusters discussed in Section 6.2.

This model, however, predicts that a cluster would consist of hectometer-scale craters, with a surrounding circular aura or elliptical strewn field of small craters leading off in one direction toward a primary crater source. On Mars we have not observed this typical strewn field pattern. Clusters are generally not surrounded by an circular aura or elliptical tail of smaller craters, and in the ray-like string of secondaries in Fig. 6a, for example, there is no obvious size sorting along the axis of the string. From these observations we conclude that although the loss of smaller craters may be aided by drag, it requires additional effects.

As a third process, therefore, we now examine fragmentation of the smaller fragments of the ascending, dissociating ejecta block. Popova et al. (2003) (Fig. 5) noted that strong rocks with dimensions of a few meters (crushing strength ~25 bars, as with ordinary chondrites) can survive passing through the present martian atmosphere without breaking, but weak rocks (strength ~1 bar, comparable to carbonaceous chondrites) of this size do not survive. From that result, we suggest that much of the loss of smaller craters from the cluster comes from fragmentation of weak blocks in the swarm, both during ascent and decent.

To summarize so far, we assume that sufficiently large primary impact craters loft few hundred m scale blocks at speeds up to at least 3–4 km/s, but that these blocks are highly fractured during the launch process from the primary crater. In the lunar case, such blocks maintain integrity, but with atmospheric drag stresses, the fractures cause them to dissociate immediately into smaller (meter- to decameter-scale) bodies. Pieces initially in the general size regime of 4 to 12 m not only suffer drag but are themselves weak enough that many are fragmented during ascent through of the martian atmosphere, and lost to the swarm. The remaining larger fragments move upward in a swarm.

Bodies in the swarm dissociate with lateral separation velocities of the order 10 m/s, as discussed in Section 3. During the tens of minutes of suborbital flight, the swarm spreads to characteristic diameters of 5, 10, 20, or 30 km before descent. Additional fragmentation and loss of small, fractured weak rocks of $d \lesssim 12$ m may occur during descent. The swarm thus creates upon impact a cluster of craters of diameters around 40 to 500 m or more, spread over a patch of the dimensions just mentioned—as observed.

6.3. Relationship to rays

The existence of bright rays around lunar and other craters shows that initial launch conditions produce tight azimuthal clustering of high-velocity jets of ejecta. These may play a key role in launching the highest velocity blocks, but the ultimate cause of these jets is not well understood. Theories of fragment formation based on the Z-model formalism of Maxwell and Seifert (1975) can explain distribution of fragments by sizes and velocities (Ivanov, 2000), but do not adequately explain either the highest-velocity part or the high directionality of some fragment streams. Many lunar rays contain dis-

crete, though ragged, clumpings of craters, proving that substantial blocks with individual identities are included in the azimuthally-focused jets.

On the Moon, the brightness of rays may be associated with the disturbance of underlying fresh surface material (less affected by space weathering) and/or the addition of finely comminuted secondary material. Pieters et al. (1985) found evidence that the brightness of the Copernicus rays is due to the deposition of highland ejecta mixed with local mare basalt. Analyses of near-IR reflectance spectra, multispectral imagery, and a variety of radar data by Hawke et al. (1996, 1999) suggest that a Tycho ray in Mare Nectaris, 350–550 km from the 41-km impact crater, involves fresh material excavated by secondary debris, and the same is true in other Tycho ray segments. This supports early work on secondaries and ray formation by Shoemaker (1962).

Classic bright "rays" at large scale are rare on Mars because the fine material associated with albedo effects are quickly disturbed by martian atmospheric deposition and mixing of dust. THEMIS nighttime infrared images, however, reveal several ray systems by their thermal properties. Hectometer-scale ray systems are common around some fresh, small, martian craters, which are much younger in age than the average large craters. Figs. 6b and 6c, as well as THEMIS imagery, confirm association of cluster-like ejecta blocks and secondary crater groupings with ray-like streamers of coarse martian material. While most recognizable secondaries are located at modest distances from the rim of primary craters, some are formed at great distances. Rays from the lunar crater Tycho are as long as 1500 km. As noted earlier, McEwen et al. (2005) traced martian secondary craters as far as 800–1600 km from a 10-km primary, Zunil, in the area of the young plains of Elysium. Additional examples of martian rayed craters were identified by Tornabene et al. (2005). They listed four km-sized craters (2–7.4 km) with maximal measurable ray length of about 600 km. Distant secondaries are not surprising, in view of the fact that we have martian rocks in our museums launched at >5 km/s. To summarize, both martian and lunar examples confirm our earlier conclusion that fragments can be launched at high speed and can fly for hundreds of seconds before re-impacting Mars (see also Schultz, 1986).

The string of craters in Fig. 6 presents several intriguing details which may support our model. The fact that it has a width of only ~3–5 km (Fig. 6a), somewhat less than most clusters, may be a result of the fact that well-defined rays lie closer to their parent primary clusters than most of our clusters, and hence have less flight time for the lateral velocity to separate the fragments. In the same way, the fact that the size distribution in the secondary string (Fig. 6d, solid symbols) shows a less well-defined bell curve than found among the clusters might be associated with less flight time for the smallest material to be winnowed by the atmosphere, although the modeling of drag-induced separation of small fragments deserves more work. The difficulty of seeing a prominent bell-curve shape for the grouping, such as shown in Fig. 7, may also be due to the high density of background craters, shown by open symbols. Comparison of the solid and open symbols suggests the cluster

craters become best defined as $D \gtrsim 125$ m, consistent with our other data.

6.4. Details of high-velocity launch: spallation theory

High velocity blocks are believed to be launched most efficiently by spallation of the coherent rock layers near the point of the intersection of the shock wave with free surface. Initial velocity of ejecta fragments is proportional to the velocity of the matter behind the shock wave, so it decreases with the distance from the impact point. A simple analytic theory of spallation due to interference of the shock wave with the free surface was proposed by Melosh (1984, 1985, 1989) and was applied for explanation of the martian "SNC" and lunar meteorites found at the Earth. In a simplified form this model is as follows.

The impact induced shock wave propagates as from a spherical explosion but with the effective center of energy release located at some depth d_{eff}. This depth may be estimated as about projectile size, so $d_{eff} \sim d$ (Melosh, 1989, Chapter 5), although it may vary depending on target and projectile properties. In the case of plane compression, the elastic wave meeting the free surface perpendicularly, a plane elastic wave of rarefaction is formed. The near surface zone is strongly influenced by rarefaction. The formation of a spallation layer is possible in the zone of interference of the compression and rarefaction waves. This layer will move as a solid body, if the shock wave amplitude is not very large. The final velocity of spalls (i.e., ejected rock fragments), v, is equal to twice the velocity of the matter u behind the infalling shock wave (Melosh, 1984, 1989).

The velocity after the shock wave produced by impact may be estimated as $u = 0.5AV(d/2r)^{1.87}$ (Melosh, 1984), where A is the numerical factor of the order of unity, V is the impact velocity, d is the projectile diameter, r is the distance from the effective center. Melosh suggests that high velocity blocks are formed at the first stages of crater formation, before the main volume of the total ejecta is thrown out the crater. At small distances from the epicenter ($\sim d$ from the impact point $r \sim \sqrt{2}d_{eff}$), the velocity is about $u \sim 0.15V \sim 1.5$ km/s. So the spalls will attain ejection velocity $v \sim 2u \sim 3$ km/s. The thickness of the spallation layer is usually estimated as $z_s \sim \sigma d/(\rho c v) \sim 0.01$–$0.02d$ for assumed strength about 0.1 GPa, or 0.3–0.6d for $\sigma \sim 3$ GPa, and ejection velocity about 1 km/s and smaller for larger velocities (Melosh, 1984). The estimates given by Melosh, however, do not describe the area close to the impact size where strong nonlinear effects may play role.

Due to 2D–3D geometry of the real impact, the shock wave meets the free surface at some angle α between the direction from the effective center of explosion and the radius from the impact point at the surface. The latter is defined by the ratio d_{eff}/r, i.e., $\sin\alpha = d_{eff}/r$. The angle of ejecta β is approximately equal to twice the angle α. For $r \gg d_{eff}$, we obtain $\beta = 2\alpha = 2d_{eff}/r$. As radius r increases, angles α and β decrease. The spallation layer is twisted and becomes fragmented, and the disrupted material is ejected as blocks.

According to Melosh (1984), the elevation angle of the ejecta is a function of rock strength and the Poisson ratio. It is nearly vertical close to the impact and decreases at greater

distances; it is about 30–70° at the distances ∼1–4d from the epicenter (Melosh, 1984, Fig. 6).

The upward directed component of the ejecta velocity is approximately equal to twice the velocity component behind the shock wave perpendicular to the initial surface, while the horizontal component is approximately equal to the horizontal component of the velocity behind the shock wave. The vertical velocity decays faster with radial distance than the horizontal velocity. Only close to the epicenter will we have sufficiently large velocity to create clusters. It is possible to estimate the distance from impact point where the spall velocity will be large enough to eject material with suborbital velocity. Taking into account decay of the velocity after shock as $r^{-1.87}$ (given above) and some average angle of ejecta, one may estimate that the spall velocity exceeds 1 km/s up to the distances about 1.1d from impact point (along the surface) for 10 km/s impact. This is conservative estimate because it predicts spall velocities exceeding V_{esc} at the distances smaller than the projectile size. Numerical modeling of 10 km/s impacts (Head et al., 2002; Artemieva and Ivanov, 2004; see below) demonstrated that spall velocity >1.5 km/s may extend up to 1–2 d from the impact point. We note that for high velocity impactors, vaporization of part of the projectile or ground ice may be important near the impact point, and gas pressure may cause additional spreading of ejecta particles.

At large distances the spallation layers are thicker than near the impact point, but the velocity is smaller, and the angle of ejection is smaller. At some distance from the impact point the spallation ceases. According to Melosh (1984), the spalls are broken off as thin plates. He estimated the aspect ratio of the spalls (∼10–20), taking into account the velocities imposed on the fragment at the instant of its ejection. The spalls have a larger velocity on the end nearest to the impact site. Taking into account this high aspect ratio (∼10), the spall size needs to be converted into the mean fragment size, i.e., the diameter of a sphere whose volume equals the volume of the spall plate. The mean fragment size is about 0.1d. The mean fragment diameter normalized by the projectile diameter and target strength is strongly dependent upon the depth of penetration, d_{eff}/d (Melosh, 1984). The numerical simulations (Artemieva and Ivanov, 2004, see below) demonstrate that the highest velocities ($v > 1$–3 km/s) occur in the surface layer with thickness about 0.4d. Additionally, the study of secondary craters by Vickery (1986) demonstrated that maximum inferred ejecta sizes are much greater than the maximum predicted high-velocity spall sizes. In other words, nearby secondaries should be larger than distant, high velocity secondaries, as actually observed (see Section 6.6 below). We will use spall layer thickness $z_s \sim 0.1$–0.4d in our estimates. This thickness combined with extension of spall layer allows to estimate the volume of high velocity ejecta A_{ej} as about ∼0.7–2.9 of projectile volume A_p that coincides with estimate made in Section 1.

According to our model, we need to launch high-velocity blocks initially of $d \sim 300$–400 m size into space, so that they can break up into adequate numbers of 10- and 20-m scale pieces, and a few bigger pieces (with the largest piece typically as big as 100–150 m), to make the observed clusters. It

seems reasonable that plates with high aspect ratio will break into blocks of dimension ∼z_s during ejection with high velocity. Thus to spall off blocks of, say, 300–400 m would require an impactor at least 750–4000 m across. Using $D/d = 21$ (from Section 2.3), this suggests parent craters in a size range of larger than 15 to 84 km.

The ejected rocks formed in the spallation layer are not subjected to high pressure, contrary to the material in the main excavation flow. The interaction of stress and rarefaction waves near the free surface causes the formation of spalls, which may be further disrupted into separate fragments due to difference of velocities across the surface or due to stored elastic stresses (Melosh, 1989).

Ejection of spall debris occurs with velocities close to the escape velocity, but in our model such blocks would be severely fragmented, which helps explain the immediate breakup and beginning of lateral spreading of the block into a swarm of fragments that causes a crater cluster. Among blocks that land close to the primary crater, the flight time and spreading are inadequate to create a cluster of individual craters hundreds of meters apart. We note that such close-in secondaries are often seen to have irregular shapes, consistent with impact of a tight swarm of fragments.

Launch velocities of about 3–5 km/s, needed to eject fragmenting blocks to large distances and create relatively isolated clusters, can be attained only at rather small distances from the epicenter. Head et al. (2002, Fig. 2) show 3 km/s velocities attained at a distance of three projectile radii, in an impact with velocity 10 km/s. Qualitatively these results are consistent with Melosh's (1984, 1989) theory, but additional insights may come from direct numerical simulations. O'Keefe and Ahrens (1986) calculated oblique and normal impacts of silicate projectiles onto a silicate half space to determine whether the gas produced in shock vaporization of projectile and planetary material could entrain and accelerate surface rocks, thus providing a mechanism for MM launch. At plausible impact velocities, vapor plume jets are produced at oblique impact angles of 25° to 60° and have speeds as great as 20 km/s. These plumes flow nearly parallel to the planetary surface. With impacts of projectiles having radii of 0.1 to 1 km, the resulting vapor jets have rather high densities and can, in principle, entrain modest sized martian surface rocks and accelerate them to velocities 5 km/s.

Ivanov and Artemieva (2001) made 3D numerical simulations to study MM launch. For impact velocities of 15 to 20 km/s and impact angles of 30° to 60° to the horizontal, the mass of unmelted particles with the velocity above 5 km/s is about 5% of the impactor mass. The action of vaporized material may be important in moving ejecta through the atmosphere. For impact angles of 40°, and especially 30°, the stream of unmelted, low-shocked material moves at a low angle to the surface, at the leading part of the ejecta curtain. Strength, layering, and realistic fragment size distributions were not fully taken into account in these simulations. Additional numerical simulations of oblique impacts onto Mars have been published by Artemieva and Ivanov (2002, 2004). Their subject is once more MM launch, but information on formation of high-velocity ejecta can be extracted. In the simulation of a

200-m diameter impact or with the velocity 10 km/s at an angle of 45°, the distributions of ejection velocity at different depth and distances show that the thickness of high-velocity spallation zone ($V_{\text{ejecta}} > 5$ km/s) is about $0.2d$ and this zone extends to the distance 1–$2d$ from the impact point. Ejecta velocities exceeding 1–3 km/s occur in the layer with thicknesses up to $0.4d$. These target layers have moderate compression (about 10–45 GPa) that agrees with the stress level of MMs. The crucial question is the size distribution of ejected fragments. The disruption process is not included in the hydrocode, so the simplified approach was used. The maximal size of fragments considered by Artemieva and Ivanov (2004) is about 10–30 cm, i.e., smaller than the blocks we need to create clusters. It is important to note that large intact blocks may have different size distributions and different maximum sizes than considered by Artemieva and Ivanov (2004). Much larger fragments may be formed in the spallation zone (see Section 6.6 below).

To summarize, current theory, combined with direct observation of secondary craters, suggests that large blocks may be thrown to large distances on Mars during sufficiently large impacts, but further modeling is needed to clarify the process.

6.5. Comment on size distribution of martian meteorites

MM data must be fitted consistently into our picture of fragment launches from Mars. Eugster et al. (2002) tabulate their krypton isotope data on seven MMs found on Earth, giving minimum Earth-atmosphere entry diameters of 0.44 to 0.50 m for all seven. They also mention measurements of two other MMs using other isotopic systems, giving minimum pre-atmosphere diameters of 0.4 to 0.8 m. On the other hand, there cannot be too many pre-atmosphere rocks much larger than a few meters, or we would expect to see more meteorites that were buried at deeper depths in their parent object and shielded from cosmic rays. Eugster and others discuss ejecta in terms of "mean sizes" of blocks, and such terminology has led to a perception that only small (sub-meter scale) rocks are launched off Mars. As seen above, this is inconsistent with our observations of clusters of 300-m-scale craters. There is some controversy over whether MMs were launched off Mars with these small sizes or were larger blocks that were fragmented in space, perhaps during aphelion passages through the asteroid belt (Nyquist et al., 2001); most are believed to have been directly delivered to Earth, given the cosmic ray exposure ages of no more than 20 Myr (Nyquist et al., 2001).

The emphasis on small blocks in some literature (Eugster et al., 2002; Artemieva and Ivanov, 2004) might seem to suggest that ejected meteoritic blocks are mostly $\leqslant 1$ m in size. However, an apparent contradiction is that the narrow range of observed MM entry sizes is consistent with the steep power-law distribution of sizes in fragmentation events (Hartmann, 1969). To speak of "mean sizes" is misleading; most particles are in the smallest diameter bins, but there can be a few much larger bodies if primary impact events are large enough. With a typical power-law size distribution for secondary ejecta fragments, with log-incremental number roughly proportional to $D^{-3.5}$, the number of objects with sizes from 1/2 to 1 m would be

of order 11 times as great as the number with sizes from 1 to 2 m. Earth-atmosphere survival below such sizes is also inhibited. Thus, the MMs we are most likely to see are at the small end of the initial size distribution, but big enough to produce recoverable terrestrial meteorites.

6.6. Minimum size and frequency of primary craters needed to create clusters and martian meteorites

The existence of the "large crater clusters" offers opportunities to test existing theoretical models of fragment sizes launched from primary craters. When Artemieva and Ivanov (2002, 2004), in discussing MM launches, assumed that unmelted ejecta body sizes vary from microns to 10–30 cm, they based this on results of high energy explosions in rocks, referring to experimental TNT explosions with explosive mass of 500 tons. According to the discussion in Section 6.4, the minimum primary crater size to create our clusters should be larger than the size needed to launch the MMs.

Current modeling suggests that known MMs come from primary craters of minimum size 3.1 km $< D <$ 7 km, and that favorable impacts launch tens of thousands of meter-scale blocks into space (Head et al., 2002). Such craters must have formed within the last 20 Myr, based on the cosmic ray data. Head et al. (2002) propose craters of $D >$ 3 or 4 km for shergottites launched from bare rock surfaces, and 7 km for Nakhlites or Chassigny, launched from 1300 Myr-old rock layers, which may have surfaces with some meters of regolith (Hartmann et al., 2001). Data of Vickery (1986, 1987) and Hirase et al. (2004) suggest that the small blocks launched at $> V_{\text{escape}}$ may preferentially come only from the highest speed ejecta jets and from the highest speed impacts. The models suggest that larger craters are needed to launch the fragments that produce the clusters. In Section 6.4 above, we found that spallation theory requires primary meteoroids at least 0.75–4 km across to launch the block sizes we need (300–400 m) to make clusters, implying primary craters of minimum size 15–84 km across to produce our clusters.

Vickery's (1987) work suggests the possibility of still larger sizes. She studied secondaries primarily around four martian craters ($D =$ 26, 28, 145, and 227 km), out to distances corresponding only to V_{launch} of ~800 m/s for the smallest craters and 1.5 km/s for the largest (the secondaries were hard to identify confidently at larger distances). She also derived an empirical equation giving the dependence of largest fragment size on velocity of launch for each crater. Extrapolating her equation to $V = 3$ km/s, we find maximum fragment sizes of only ~40–50 m for the smaller two craters, and ~80–140 m for the larger craters. The latter size range is closer to the block size needed to make the largest clustered craters we see. This result suggests that not 13–17 km craters, but rather craters as large as 100–250 km may be needed to launch blocks large enough to make clusters. However, the error bars on Vickery's equations are such that the 26 km crater could produce blocks up to 300 m in size, and the 145 km crater could produce blocks up to 1000 m in size. In any case, the size–velocity anti-correlation mentioned in Section 6.1 requires that still larger craters are

needed to eject such large blocks to near escape velocities, implying minimum primary crater sizes of ∼30 to ∼200 km.

Further constraints are possible, from crater formation rate information. Barlow and Osborne (2001) find most clusters on Noachian and Hesperian terrain, but some of our clusters, such as the one on Meridiani Planum (Fig. 4) and others on Olympus Mons, are found on geologically young surfaces. This implies cluster formation within the last few hundred Myr, possibly within the last 20 Myr in the case of the sparsely cratered surface of Meridiani Planum, which may have been exhumed within the last tens of Myr (based on paucity of small sharp craters; Hartmann et al., 2001; Hartmann, 2005). These results suggest clusters accumulating on surfaces throughout martian history. Note that it is plausible that many young clusters on Mars might be products of a single large impact. The numbers currently thus imply that Mars should have at least one or more craters big enough to have formed clusters ($D > 17$ km or perhaps $D > 100$ km) within the last 20–300 Myr.

The catalog of martian craters maintained by Barlow (2005) allows investigation of this issue. Consistent with our implication, Barlow (private communication) lists statistics for craters with visible layered or radial ejecta. She lists 27 craters of $D > 17$ km and one crater of $D > 100$ km in the Upper Amazonian alone; for the whole Amazonian she lists 109 craters of $D > 17$ km and one crater of $D > 100$ km. These numbers appear consistent with our observation of widespread large crater clusters, including some on stratigraphically young units. (If the entire Amazonian represents the last 2000–3000 Myr, the number of $D > 17$ km craters in the last 300 Myr would be estimated as ∼ 10–16.) It seems plausible that one or a few large craters scattered the clusters seen on the youngest stratigraphic units. As better statistics become available on the distribution of large clusters, this approach could be refined.

A second approach to the problem is possible. Existing estimates of martian cratering rates allow estimates of the rates of formation of craters larger than a given diameter. Head et al. (2002) estimate a formation interval of 1 every 0.2 Myr for 3-km craters for the whole planet Mars. Hartmann (2005) gives an updated iteration of his own crater isochron system showing a similar result, with a formation interval of ∼0.1 Myr at all craters of $D > 3$ km, but ∼0.5 Myr at $D > 7$ km. These numbers would predict 40 to 200 MM launch events from Mars in the last 20 Myr—many more than observed on Earth. However, Head et al. (2002) and Hartmann and Barlow (2006) resolve this problem by positing that only about 10% to 40% of the martian surface has intact igneous rocks close enough to the surface to produce the observed types of meteorites. This would reduce the number of launches to as little as 4 to 50 in the last 20 Myr, overlapping the currently known number of 3 to 7 MM launch sites from young igneous rocks during that period. Our numbers would weakly favor the idea that MMs come from craters closer to 7 than 3 km, and/or that geologic surface units capable of efficient launch cover considerably less than half of Mars.

Given the above order-of-magnitude agreement, we can make an argument about the size of primaries needed to make the large clusters. From the impact rates derived in Hartmann (2005), the impact interval for craters larger than 15, 100, and

200 km would be of the order 1.5, 100, and 400 Myr for the whole planet, respectively. The fact that we appear to have clusters on surfaces only tens of Myr old, or less, favors craters smaller than 100 km as the limiting size for cluster production, barring a statistical fluke. Craters 70 km across, for example, appear to form about once every 40 Myr from the statistics we are using.

Longer time periods would be required to accumulate all the clusters we see, especially the largest ones. Barlow and Osborne (2001) estimated that most of their clusters (larger than ours) dated from the Hesperian and Noachian, when the cratering rate was larger than it is today. Putting these arguments together, we suggest that the parent primary craters of crater clusters probably have $D > 84$ km, possibly as low as 15 km, and that large crater clusters are not all ancient features.

6.7. Role of inhomogeneities and asymmetries

In any attempted analysis of ejection physics we must keep in mind that crater-forming explosions are not idealized, radially symmetric events. The existence of ray systems immediately proves this. In addition, the target area may be inhomogeneous as an initial condition, due to previous impacts of secondaries and primaries. Ejection of blocks is probably affected by local layering (lava flow history, subaerial deposition, ground ice and aquifer history?). It is favored by a near-surface solid rock layer, such as an intact lava flow, and hindered by unbonded particulate material, which attenuate shock waves (Head et al., 2002). These issues deserve further treatment in all studies of launch of planetary material.

7. Conclusions

We have identified two types of craters clusters on Mars. Small clusters involve craters with diameter D up to a few tens of m spread over typically 100–300 m, and form due to breakup of weak "primary meteoroids" from interplanetary space during passage through the martian atmosphere (cf. Popova et al., 2003). Large clusters involve craters with $D = 70$–900 m spread over 5 to 30 km.

Our favored model of the formation of large crater clusters is as follows. The clusters require swarms of fragments with typical sizes of 5 to 50 m, but are deficient in fragments smaller than about 12 m, and show extreme losses below 4 m. The fragments come from a few-hundred m blocks of secondary debris spalled and ejected at ∼3 km/s $< V < 5$ km/s from martian impact craters probably in the size range $D \gtrsim 85$ km, though possibly as small as 15 km. Existence of such blocks is supported by Vickery (1986, 1987). In our scenario, the blocks are typically very weak upon launch and begin to break up and spread into a swarm of fragments during ascent. This necessary interaction with the martian atmosphere explains why we do not see similar crater clusters on the Moon.

The lateral velocity of spreading of the fragments of large ejected blocks is about $u = 5$ to 8 m/s for ejection velocity $V = 3$–5 km/s and density $\rho_m = 2.5$ g/cm^3 [Eq. (1)]. For flight duration 1000–2000 s, the dispersion of fragments across

the trajectory $\Delta r = 5$–16 km, explaining typical cluster sizes. Occasional larger clusters, as observed, could be obtained for longer suborbital flight that may last for 5000 s. For such a long flight, cluster width could range up to $\Delta r \sim 25$ km, explaining clusters such as seen in Meridiani Planum (Fig. 4). The flight distance crossed along the trajectory for $V = 3$ km/s would be $\sim$1500 km, making it difficult to identify the parent crater. Conversely, as noted above, the ray-like string of secondary craters in Fig. 6 shows less lateral dispersal, as explained by its shorter flight time from its primary.

Fig. 12 shows examples of calculated scattering fields, which could be formed after launching of large secondary fragmented blocks at sub-escape velocity. A number of fragments with power-law size distribution (with slope-2) is launched with velocity 2 km/s at a 45° angle to surface. The existing martian atmosphere caused both lateral and longitudinal spreading of the projectiles. These results match the observed characteristics of the large martian crater clusters, supporting the model.

We suggest that a whole spectrum of martian secondary crater phenomena may exist, from obvious low-velocity secondaries with roughly power-law size distributions, near primaries (which are out of the scope of this paper), to more distant secondary clusters in ray-like alignments (similar to Fig. 6), to scattered random clusters with more bell-curve-like size distributions (Fig. 4). Launch of large, weak secondary bodies at near-escape velocities appears to explain many properties of large clusters.

Questions are raised for future research, especially regarding the features of the spallation layer, the detailed mechanism of production, and breakup of ascending secondary fragments from craters. The role of volatiles in such fragments, vis-à-vis explosive breakup and lateral velocities, needs more work. To investigate further the relationship between our large clusters and the distant secondaries described by McEwen et al. (2005) and the various degrees of clustering among secondaries as described by Bierhaus et al. (2001), it would be useful to undertake more complete surveys of large clusters. In particular, we suggest more careful study of the relation of our large clusters to ray systems, and obvious strings of secondaries, such as illustrated in our Fig. 6. Studies of such secondary strings, and clumps of craters among them, may shed more light on the breakup of secondary debris during flight. Broader surveys may reveal association of seemingly isolated large clusters with nearby strings of secondaries of specific large primary source craters hitherto unrecognized.

The same model relates to the production of MMs. The crater statistics of Hartmann (2005), Hartmann and Neukum (2001), and Neukum and Ivanov (1994) grossly support the idea that MMs come from the high velocity members of ejecta from (high impact-velocity?) craters of $D > 3$ to 7 km, as per Head et al. (2002). Our analysis indicates that the large crater clusters come from ejecta from considerably larger craters.

Salient results on related topics can be summarized:

(1) Existing models and observations are consistent with weak meteoroids breaking up in the martian atmosphere and
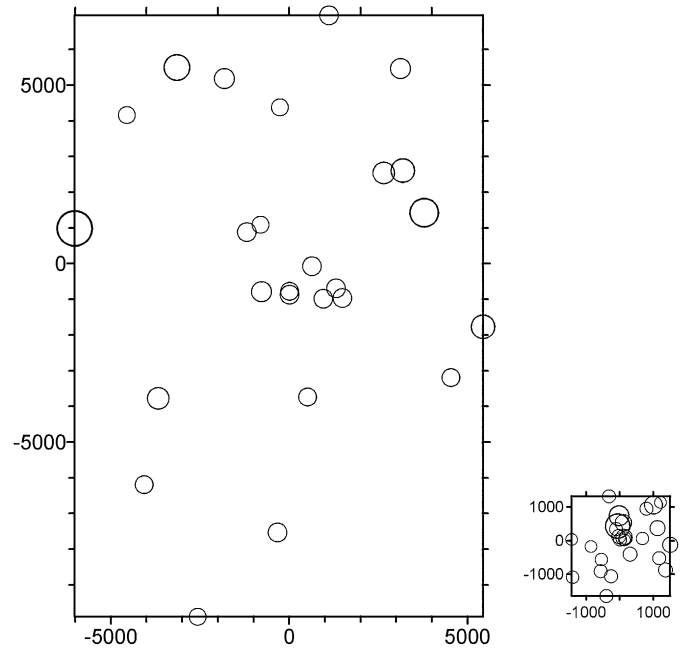

Fig. 12. Simulation of large cluster of craters, assuming ejection of large, secondary fragmented blocks of material launched at sub-escape velocity out of impact craters. During their flight through the atmosphere they could separate to the spacings required to create such large crater clusters (cf. Figs. 2–6). Model results depends on suggested initial condition (velocity, fragment size distribution, etc.). Launch velocity $V = 2$ km/s in left panel, 1 km/s in right panel; note different scales.

spreading at lateral velocities of $u =$ tens of m/s, causing the observed "small clusters."

(2) Theoretical models give some suggestion that weak cometary bodies could break up and produce small fragments spreading at higher velocities of $u > 100$ m/s. These might produce some of the most dispersed "small clusters."

(3) The present models of primary meteoroid entry fail to produce conditions that would explain our "large clusters" of 500 m craters spread over 5–30 km. Furthermore, we see no smooth continuum between the small and large clusters; they seem to represent two distinct phenomena.

(4) The size distribution of many large clusters appears inconsistent with the normal power-law spectrum expected for most types of fragmentation events, and has an unusual concentration of craters at about 70–900 m sizes, and a shortage of craters in $D \lesssim 100$–200 m relative to normal power-law fragment distributions.

(5) This size distribution could suggest a breakup of rubble-pile asteroids or of comets, hypothesized by Weidenschilling et al. (1997) to be composed of icy planetesimals of the order 10^2 m size. However, we have been unable to show how such bodies could disperse rapidly enough to produce the cluster sizes observed.

(6) More studies are needed of the spallation process, lateral separation of meteoroid fragments, and the possible influence of volatiles in producing higher lateral separation velocities than in current models, which neglect volatile effects.

(7) Our figures are consistent with the idea that most MMs are probably launched by martian craters $\succeq$ 3–7 km across, as suggested by Head et al. (2002), but somewhat favoring the larger sizes.

Acknowledgments

References

Artemieva, N.A., Ivanov, B.A., 2002. Ejection of martian meteorites—Can they fly? Lunar Planet Sci. XXIV. Abstract 1113.

Artemieva, N.A., Ivanov, B.A., 2004. Launch of martian meteorites in oblique impacts. Icarus 171, 84–101.

Artemieva, N.A., Shuvalov, V.V., 1996. Interaction of shock waves during the passage of a disrupted meteoroid through the atmosphere. Shock Waves 5, 359–367.

Artemieva, N.A., Shuvalov, V.V., 2001. Motion of a fragmented meteoroid through the planetary atmosphere. J. Geophys. Res. 106, 3297–3310.

Asphaug, E., Melosh, H.J., 1993. The Stickney impact of Phobos: A dynamical model. Icarus 101, 141–164.

Baldwin, B.S., Sheaffer, Y., 1971. Ablation and breakup of large meteoroids during atmospheric entry. J. Geophys. Res. 76, 4653–4668.

Barlow, N.G., 2005. A review of martian impact crater ejecta structures and their implications for target properties. In: Kenkmann, T., Hörz, F., Deutsch, A. (Eds.), Large Meteorite Impacts. In: Geological Society of America Paper, vol. 384. Geological Society of America, Boulder, CO, pp. 433–442.

Barlow, N., Osborne, P., 2001. Searching for isolated crater clusters on Mars. Lunar Planet. Sci. XXXII. Abstract 1602.

Bierhaus, E.V., Chapman, C.R., Merline, W.J., Brooks, S.M., Asphaug, E., 2001. Pwyll secondaries and other small craters on Europa. Icarus 153, 264–276.

Borovička, J., Kalenda, P., 2003. The Morávka meteorite fall: 3 meteoroid dynamics and fragmentation in the atmosphere. Meteorit. Planet. Sci. 38, 1023–1043.

Borovička, J., Spurný, P., 1996. Radiation study of two very bright terrestrial bolides and an application to the Comet S-L 9 collision with Jupiter. Icarus 121, 484–510.

Borovička, J., Popova, O.P., Nemtchinov, I.V., Spurný, P., Ceplecha, Z., 1998. Bolides produced by impacts of large meteoroids into the Earth's atmosphere: Comparison of theory with observations. I. Benešov bolide dynamics and fragmentation. Astron. Astrophys. 334, 713–728.

Borovička, J., Spurný, P., Ceplecha, Z., 2001. The Morávka meteorite fall: Fireball trajectory orbit and fragmentation from video records. Meteorit. Planet. Sci. Suppl. 36. A25.

Bottke, W.F., Melosh, H.J., 1996. Binary asteroids and the formation of doublet craters. Icarus 124, 372–391.

Costard, F., Forget, F., Mangold, N., Peulvast, J.P., 2001. Formation of recent martian debris flows by melting on near-surface ground ice at high obliquity. Science 295, 110–113.

Dessler, A.J., 1991. The small comet hypothesis. Rev. Geophys. 29, 355–382.

Docobo, J.A., Ceplecha, Z., 1999. Video record (CD copy attached) of the Spain bolide of June 14, 1996: The atmospheric trajectory and orbit. Astron. Astrophys. Suppl. 138, 1–9.

Eugster, O., Busemann, H., Lorenzetti, S., Terribilini, D., 2002. Ejection ages from krypton-81–krypton-83 dating and pre-atmospheric sizes of martian meteorites. Meteorit. Planet. Sci. 37, 1345–1360.

Frost, M.J., 1969. Size and spatial distribution in meteoritic showers. Meteoritics 4, 217–232.

Greeley, R., Guest, J., 1987. Geologic map of the eastern equatorial region of Mars. Map I-1802-B. U.S. Geologic Survey, Reston, VA.

Hartmann, W.K., 1969. Terrestrial, lunar, and interplanetary rock fragmentation. Icarus 10, 201–213.

Hartmann, W.K., 1999. Martian cratering VI. Crater count isochrons and evidence for recent volcanism from Mars Global Surveyor. Meteorit. Planet. Sci. 34, 167–177.

Hartmann, W.K., 2005. Martian cratering 8: Isochron refinement and the chronology of Mars. Icarus 174, 294–320.

Hartmann, W.K., Barlow, N., 2006. Nature of martian uplands: Effect on martian meteorite age distribution and secondary cratering. Meteorit. Planet. Sci. 41, 1453–1468.

Hartmann, W.K., Engel, S., 1994. Martian atmospheric interaction with bolides: A test for an ancient dense martian atmosphere. Lunar Planet. Sci. XXV. Abstract 511–512.

Hartmann, W.K., Neukum, G., 2001. Cratering chronology and evolution of Mars. In: Kallenbach, R., Geiss, J., Hartmann, W.K. (Eds.), Chronology and Evolution of Mars. International Space Science Institute, Bern, pp. 165–196; also in Space Sci. Rev. 96 (2001) 165–194.

Hartmann, W.K., Anguita, J., de la Casa, M.A., Berman, D.C., Ryan, E.V., 2001. Martian cratering 7: The role of impact gardening. Icarus 149, 37–53.

Hawke, B.R., Blewett, D.T., Bell III, J.F., Lucey, P.G., Campbell, B.A., Robinson, M.S., 1996. Remote sensing studies of lunar crater rays. Lunar Planet. Sci. XXVII. Abstract 507.

Hawke, B.R., Blewett, D.T., Lucey, P.G., Peterson, C.A., Bell, J.F., Campbell, B.A., Robinson, M.S., 1999. The composition and origin of selected lunar crater rays. In: Workshop on New View of the Moon II: Understanding the Moon through the Integration of Diverse Dataset, Flagstaff, AZ, September 1999. Lunar and Planetary Institute, Houston, TX. Abstract 8035.

Head, J.N., Melosh, H.J., Ivanov, B.A., 2002. Martian meteorite launch: High-speed ejecta from small craters. Science 298, 1752–1756.

Holsapple, K.A., 1994. Catastrophic disruptions and cratering of Solar System bodies: A review and new results. Planet. Space Sci. 42, 1067–1078.

Housen, K.R., Schmidt, R.M., Holsapple, K.A., 1983. Crater ejecta scaling laws—Fundamental forms based on dimensional analysis. J. Geophys. Res. 88, 2485–2499.

Hirase, Y., Nakamura, A.M., Michikami, T., 2004. Ejecta size–velocity relation derived from the distribution of the secondary craters of kilometer-sized craters on Mars. Planet. Space Sci. 52, 1103–1108.

Ivanov, B.A., 1991. Mechanical consequences of impact formed Stickney on Phobos. Lunar Planet. Sci. XXXII. Abstract 619–620.

Ivanov, B.A., 2000. The model for secondary crater's distribution. Lunar Planet. Sci. XXXI. Abstract 1782.

Ivanov, B., 2001. Mars/Moon cratering rate ratio estimates. In: Kallenbach, R., Geiss, J., Hartmann, W.K. (Eds.), Chronology and evolution of Mars. International Space Science Institute, Bern, pp. 87–104.

Ivanov, B.A., Artemieva, N.A., 2001. How oblique should be impact to launch martian meteorites? Lunar Planet Sci. XXXI. Abstract 1309.

Lorenz, R.D., 2000. Microtektites on Mars: Volume and texture of distal impact ejecta deposits. Icarus 144, 353–366.

Maxwell, D., Seifert, K., 1975. Modeling of cratering. Close-in displacements, and ejecta. Defense Nuclear Agency, Report #DNA 3628F, Washington, DC, 101 pp.

McEwen, A.S., Preblich, B.S., Turtle, E.P., Artemieva, N.A., Golombek, M.P., Hurst, M., Kirk, R.L., Burr, D.M., Christensen, P.R., 2005. The rayed Crater

Zunil and interpretations of small impact craters on Mars. Icarus 176, 351–381.

Melosh, H.J., 1984. Impact ejection, spallation, and the origin of meteorites. Icarus 59, 234–260.

Melosh, H.J., 1985. Ejection of rock fragments from planetary bodies. Geology 13, 144–148.

Melosh, H.J., 1989. Impact Cratering: A Geological Process. Oxford Univ. Press, New York.

Mustard, J.F., Cooper, C.D., Rifkin, M.K., 2001. Evidence for recent climate change on Mars from the identification of youthful near-surface ground ice. Nature 412, 411–414.

Nemtchinov, I.V., Popova, O.P., 1997. An analysis of the 1947 Sikhote–Alin event and a comparison with the phenomenon of February 1, 1994. Solar Syst. Res. 31, 408–420.

Nemtchinov, I.V., Svetsov, V.V., Kosarev, I.B., Golub', A.P., Popova, O.P., Shuvalov, V.V., Spalding, R.E., Jacobs, C., Tagliaferri, E., 1997a. Assessment of kinetic energy of meteoroids detected by satellite-based light sensors. Icarus 130, 259–274.

Nemtchinov, I.V., Shuvalov, V.V., Kosarev, I.B., Artemieva, N.A., Trubetskaya, I.A., Svetsov, V.V., Ivanov, B.A., Loseva, T.V., Neukum, G., Hahn, G., de Niem, D., 1997b. Assessment of Comet Shoemaker–Levy 9 fragment sizes using light curves measured by Galileo spacecraft instruments. Planet. Space Sci. 45, 321–326.

Nemtchinov, I.V., Kuzmicheva, M.Yu., Shuvalov, V.V., Golub', A.P., Popova, O.P., Kosarev, I.B., Borovička, J., 1999. Šumava meteorid—Was it a small comet? In: Svoren, J., Pitch, E.M., Rickman, H. (Eds.), Evolution and Source Regions of Asteroids and Comets, vol. II. In: Proc. IAU Colloq., vol. 173. Astron. Inst. Slovak Acad. Sci., Tatranska Lomnica, pp. 51–56.

Neukum, G., Ivanov, B.A., 1994. Crater size distributions and impact probabilities on Earth from lunar, terrestrial-planet, and asteroid cratering data. In: Gehrels, T. (Ed.), Hazards Due to Comets and Asteroids. Univ. of Arizona Press, Tucson, AZ, pp. 359–416.

Nyquist, L.E., Bogard, D.D., Shih, C.-Y., Greshake, A., Stöffler, D., Eugster, O., 2001. Ages and geologic histories of martian meteorites. In: Kallenbach, R., Geiss, J., Hartmann, W.K. (Eds.), Chronology and Evolution of Mars. International Space Science Institute, Bern, pp. 105–164.

O'Keefe, J.D., Ahrens, T.J., 1986. Oblique impact—A process for obtaining meteorite samples from other planets. Science 234, 346–349.

Passey, Q., Melosh, H.J., 1980. Effects of atmospheric breakup on crater field formation. Icarus 42, 211–213.

Pieters, C.M., Adams, J.B., Mouginis-Mar, P., Zisk, S.H., Smith, M.O., Head, J.W., McCord, T.B., 1985. The nature of crater rays: The Copernicus example. J. Geophys. Res. 90, 12393–12413.

Popova, O.P., Nemtchinov, I.V., Shuvalov, V.V., Kosarev, I.B., 1999. Large meteoroids disruption at high altitude. In: Proc. Asteroids, Comets, Meteors. Abstract 10.03.

Popova, O.P., Nemtchinov, I.V., Hartmann, W.K., 2003. Bolides in the present and past martian atmosphere and effects on cratering processes. Meteorit. Planet. Sci. 38, 905–925.

Schultz, P.H. 1986. Exotic components at Apollo 15: A relook at secondary cratering. In: Spudis, P.D., Ryder, G. (Eds.), Workshop on the Geology and Petrology of the Apollo 15 Landing Site. Lunar and Planetary Institute Workshop, Houston, TX, November 1986. LPI Technical Report 86-03, p. 94.

Scott, D.H., Tanaka, K.K., 1986. Geologic map of the western equatorial region of Mars. Map I-1802-A. U.S. Geologic Survey, Reston, VA.

Shoemaker, E.M., 1962. Interpretation of lunar craters. In: Kopal, Z. (Ed.), Physics and Astronomy of the Moon. Academic Press, New York, pp. 283–359.

Shuvalov, V.V., Artemieva, N.A., Kosarev, I.B., Nemtchinov, I.V., Trubetskaya, I.A., 1997. Numerical simulation of the bolide phase of the impact of Comet Shoemaker–Levy 9 fragments on Jupiter. Solar Syst. Res. 31, 393–400.

Tornabene, L.L., McSwee Jr., H.Y., Moersch, J.E., Platek, J.L., Milam, K.A., Christensen, P.R., 2005. Recognition of rayed craters on Mars in THEMIS thermal infrared imagery: Implications for martian meteorite source regions. Lunar Planet. Sci. XXXVI. Abstract 1970.

Vickery, A.M., 1986. Size–velocity distribution of large ejecta fragments. Icarus 67, 224–236.

Vickery, A.M., 1987. Variation in ejecta size with ejection velocity. Geophys. Res. Lett. 14 (7), 726–729.

Weidenschilling, S.J., Spaute, D., Davis, D.R., Marzari, F., Ohtsuki, K., 1997. Accretional evolution of a planetesimal swarm. Icarus 128, 429–455.